THESIS FOR THE DEGREE OF DOCTOR OF PHILOSOPHY

Intramolecular Electronic Interactions in Photon Upconversion and Singlet Fission

Fredrik Edhborg

Department of Chemistry and Chemical Engineering
CHALMERS UNIVERSITY OF TECHNOLOGY
Gothenburg, Sweden 2021

Intramolecular Electronic Interactions in Photon Upconversion and Singlet Fission
FREDRIK EDHBORG
ISBN: 978-91-7905-589-9

Doktorsavhandlingar vid Chalmers tekniska högskola
Ny serie nr: 5056
ISSN: 0346-718X

Department of Chemistry and Chemical Engineering
Chalmers University of Technology
SE-412 96 Gothenburg
Sweden
Telephone +46 31 772 1000

Cover: Illustration of photon upconversion and singlet fission driven by solar light.

Printed by Chalmers digitaltryck
Gothenburg, Sweden 2021

Intramolecular Electronic Interactions in Photon Upconversion and Singlet Fission
Fredrik Edhborg
Department of Chemistry and Chemical Engineering
Chalmers University of Technology

Abstract

The sun provides our planet with an abundance of energy in the form of solar light – a continuous stream of photons. Increasing our direct utilization of solar energy will constitute a necessary part in our ongoing replacement of fossil fuels with energy sources free from greenhouse gas emissions. The sunlight contains a broad spectrum of photon energies, but only a fraction of the photons in this spectrum can be harvested by a solar energy device. In fact, the energy harvesting efficiency of solar energy technologies is mainly limited by the mismatch between the solar spectrum and the photon energies that the solar energy device can utilize efficiently. Photon energy conversion techniques provide a way to circumvent this mismatch by converting incoming photons of too high or too low energy to photons with energy that matches the absorption of the solar energy device, thus enabling utilization of a larger part of the solar spectrum.

Photon energy conversion includes both upconversion and downconversion. In this thesis, the photophysical processes of photon upconversion (PUC) by triplet-triplet annihilation and exciton downconversion by singlet fission (SF) have been investigated. The work presented in this thesis focuses on gaining knowledge and in-depth mechanistic understanding of the electronic interactions and excitation energy transfer events between chromophores that govern PUC and SF. More specifically, this thesis presents results from an investigation of *intra*molecular electronic interactions between chromophores within a molecular construct designed for PUC or SF. The mechanisms of *intra*molecular energy transfer between chromophores used for PUC have been investigated with respect to rate and efficiency. *Intra*molecular SF in a molecular dimer has been investigated in a detailed study of how the relative orientation of the chromophores and molecular conformational flexibility influence the kinetics of SF.

The results presented in this thesis show how the relative orientation of chromophores as well as the moiety connecting the chromophores, control the nature and magnitude of the *intra*molecular electronic coupling. This insight highlights the importance of controlling molecular orientations and conformation flexibility as a design parameter in the development of novel molecular systems for photon energy conversion. Further, it has been shown that the overall process of PUC or SF is faster in an *intra*molecular system compared to a corresponding *inter*molecular system. Finally, the work presented in this thesis has shown that careful design of molecular frameworks could enable efficient *intra*molecular PUC and SF materials, which have potential to increase the energy harvesting efficiency of solar energy technologies.

Keywords: Photon Upconversion, Singlet Fission, Excitation Energy Transfer, *Intra*molecular, Solar Energy Conversion

List of Publications

This thesis is based on the work presented in the following papers:

Paper I
Singlet and Triplet Energy Transfer Dynamics in Self-Assembled Axial Porphyrin-Anthracene Complexes: Towards Supra-molecular Structures for Photon Upconversion. Victor Gray, Betül Küçüköz, Fredrik Edhborg, Maria Abrahamsson, Kasper Moth-Poulsen and Bo Albinsson. *Physical Chemistry Chemical Physics, 2018, 20, 7549-7558*

Paper II
Singlet Energy Transfer in Anthracene–Porphyrin Complexes: Mechanism, Geometry, and Implications for Intramolecular Photon Upconversion. Fredrik Edhborg, Betül Küçüköz, Victor Gray and Bo Albinsson. *The Journal of Physical Chemistry B, 2019, 123, 9934-9943*

Paper III
Intramolecular Triplet-Triplet Annihilation Photon Upconversion in Diffusionally Restricted Anthracene Polymer. Fredrik Edhborg, Hakan Bildirir, Pankaj Bharmoria, Kasper Moth-Poulsen, Bo Albinsson. *The Journal of Physical Chemistry B, 2021, 125, 6255–6263*

Paper IV
Molecular Rotational Conformation Controls the Rate of Singlet Fission and Triplet Decay in Pentacene Dimers. Rasmus Ringström*, Fredrik Edhborg*, Zachary W. Schroeder, Lan Chen, Michael J. Ferguson, Rik R. Tykwinski and Bo Albinsson. *Submitted manuscript*

* These authors contributed equally

Contribution Report

Description of my contribution to the appended papers:

Paper I
Performed the upconversion experiments.

Paper II
Performed all spectroscopic experiments together with B.K. Analyzed the data and wrote the manuscript.

Paper III
Proposed the project based on existing compounds. Designed, planned and performed all spectroscopic experiments. Analyzed the data and wrote the manuscript.

Paper IV
Planned, designed and evaluated experiments together with R.R. Performed parts of the spectroscopic experiments and analyzed parts of the data. Performed the DFT calculations and wrote parts of the manuscript. First authorship shared with R.R.

List of Abbreviations

bTET	Triplet Energy Back Transfer
CCD	Charge-Coupled Device
DFT	Density Functional Theory
DPA	9,10-Diphenylanthracene
EM	Electromagnetic
ESA	Excited State Absorption
FRET	Förster Resonance Energy Transfer
HOMO	Highest Occupied Molecular Orbital
IR	Infrared
ISC	Intersystem Crossing
iTTA	*Intra*molecular Triplet-Triplet Annihilation
LUMO	Lowest Unoccupied Molecular Orbital
MCP-PMT	Micro-Channel Plate Photomultiplier Tube
MTHF	2-Methyltetrahydrofuran
PMT	Photomultiplier Tube
PUC	Photon Upconversion
PtOEP	Platinum-Octaethylporphyrin
RuOEP	Ruthenium(carbonyl)-Octaethylporphyrin
SAS	Species Associated Spectra
SET	Singlet Energy Transfer
SF	Singlet Fission
SVD	Singular Value Decomposition
TA	Transient Absorption
TCSPC	Time Correlated Single Photon Counting
TD-DFT	Time-Dependent Density Functional Theory
TET	Triplet Energy Transfer
TTA	Triplet-Triplet Annihilation
UV	Ultraviolet
xTTA	*Inter*molecular (external) Triplet-Triplet Annihilation
ZnOEP	Zinc-Octaethylporphyrin

Contents

1
Introduction

The sun is ultimately the energy source for virtually all living organisms on Earth. Sunlight drives the photochemical reaction in plants know as photosynthesis, which powers the entire biosphere on our planet. In fact, fossil fuels could be regarded as a form of solar energy, even though this solar energy has been accumulated and stored over millions of years. The use of fossil fuels has enabled the development of our modern society, but this has come with a cost that we now have started to realize. The emission of carbon dioxide (CO_2) from the combustion of fossil fuels has eventually led to an increasing CO_2 concentration in the atmosphere, which has started a process of global warming as a result of the enhanced greenhouse effect.[1] Because of this, the now living generations are facing one of the greatest challenges mankind has ever encountered. Addressing this challenge must include a reduction in CO_2 emission,[1] for example by replacing fossil energy with renewable and CO_2 emission free energy sources. The most natural and abundant choice for this is to use the sun as an energy source.

The potential of using the sun as an energy source is enormous – the collected energy from sunlight falling on Earth is more than enough to power our modern society. In fact, just a tiny fraction of the solar energy reaching the Earth would be enough to cover mankind´s global energy consumption,[2] but so far, the direct use of solar energy has been an almost negligible part in the world´s total energy supply.[3] One of the limiting factors in the utilization of solar energy is the efficiency of solar energy harvesting devices. This thesis focuses on the development of a method with potential to increase the energy harvesting efficiency of solar energy devices.

1.1 Solar Energy and Photon Energy Conversion

The energy from the sun is packaged in discrete light particles, called photons. The distribution of how much energy each photon carries is represented by the solar spectrum, as seen in Figure 1.1. A broad range of photon energies is covered in the solar spectrum: from the high energy ultraviolet (UV) radiation, through the visible light, to the low energy infrared (IR) radiation. In a solar energy device, the energy of the photons is harvested and transformed to other useful forms, such as electricity in photovoltaics (solar cell) or chemical energy in solar fuels production. However, the photon energies that a solar energy device can utilize efficiently does not always match the solar spectrum. This sets an upper limit for the overall energy harvesting efficiency of the device. For example, in solar fuel production it is often only the high energy UV photons that have enough energy to drive the photochemical reactions; photons which are scarce in the solar spectrum. Another example is photovoltaics, for which an upper theoretical efficiency limit was calculated by William Shockley and Hans J. Queisser in 1961, called the Shockley-Queisser limit.[4] According to their thermodynamic detailed balance, the energy

harvesting efficiency of a single band gap solar cell cannot exceed approximately 33%.[4–6] This means that about two thirds of the energy from the sun will be lost, also in a perfectly optimized solar cell. The main sources of energy loss in this calculation comes from the fact that low energy photons below the so-called band gap of the solar cell cannot be absorbed and the excess energy of high energy photons above the band gap cannot be utilized. By this, a large fraction of the energy arriving from the sun cannot be harvested due to the mismatch between the photon energies that are efficiently utilized in a solar energy device and the photon energies present in the solar spectrum. However, this also means that there is great potential for increasing the solar energy harvesting efficiency by implementation of photon energy conversion, that is, a technique for changing the energy of the incoming photons so it better matches the device of interest. Photon energy conversion can be done in both directions, both by converting low energy photons to higher energy photons, so called photon upconversion (PUC), or by splitting one high energy photon into two photons or excited states of lower energy, so called singlet fission (SF). Figure 1.1 visualizes how both PUC and SF could be used to increase the solar energy harvesting efficiency of a silicon based solar cell beyond the Shockley-Queisser limit: PUC enables harvesting of the energy from the sub-band gap photons and SF enables utilization of the excess energy of a high energy photon by splitting it into two photons or excited states. The figure also shows how PUC could be used to generate UV light from the abundance of visible light, which could be used in solar fuel production.

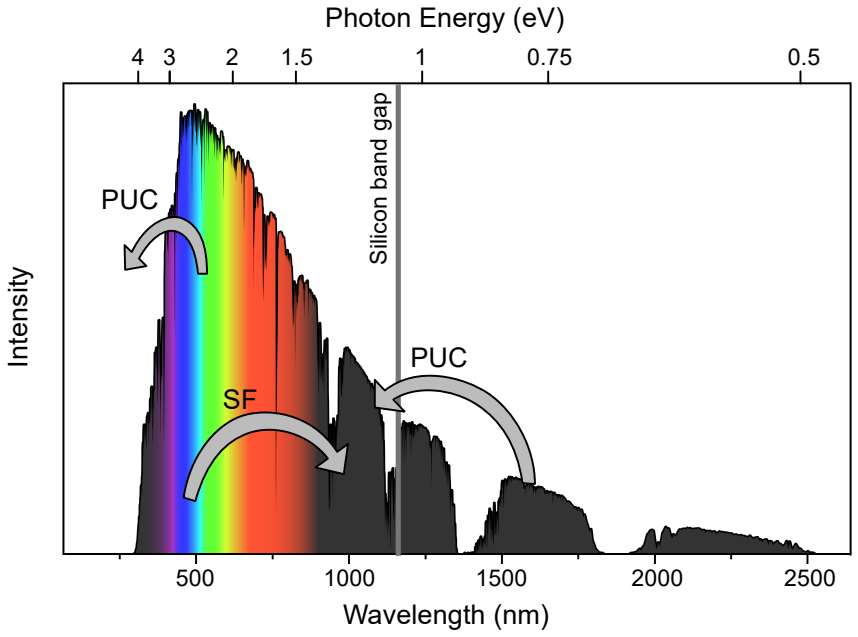

Figure 1.1: The solar spectrum at sea level. The gray line shows the band gap of silicon and the arrows show how PUC and SF could be used to increase the solar energy harvesting efficiency of a silicon solar cell. Also included is an arrow showing PUC from visible light to the UV region. Solar spectrum data from National Renewable Energy Laboratory.[7]

1.2 Photon Upconversion

Photon upconversion is a method to combine the energy of two photons to form one photon of higher energy. There are a couple of different techniques for photon upconversion, for example

two-photon absorption, second harmonic generation and triplet-triplet annihilation (TTA). Both two-photon absorption and second harmonic generation require very high light intensities. In contrast, photon upconversion by TTA can function also at lower light intensities, such as solar light. In this thesis, only photon upconversion by TTA is considered and the more general concept of PUC will from now on refer to PUC by TTA. PUC by TTA is a photophysical process where two types of molecules interact to combine the energy from two incoming photons into one emitted photon in a series of excitation energy transfer events, as will be further described in Section 2.2. The phenomena of TTA (also called triplet fusion) was first observed in 1962,[8] but the research field investigating the process started to grow around the 2000s, when it was proposed that PUC could be used to improve the efficiency of solar cells.[9–11]

In a solar cell, an upconverting material placed on the back side of the absorbing layer could increase the solar energy harvesting efficiency by catching the sub-band gap photons initially transmitted through the solar cell. For example, applying PUC to a silicon solar cell could increase its energy harvesting efficiency from ∼30% to ∼40%, which is a 33% increase in efficiency of the cell.[12,13] Further, considering that PUC could potentially be applied as an add-on feature to an existing technology, it could have a large impact on the solar energy production in the world. The add-on ability is a great advantage as it enables an easy implementation into an existing device structure.[12]

There are some examples of solar energy applications where PUC has been implemented with a proven effect from the upconversion.[14–19] However, implementation of an upconverting material into a viable product requires further development. It has been shown that PUC can reach an upconversion emission efficiency close to unity, but the best performing PUC systems are in liquid solutions where the process is governed by molecular diffusion,[20,21] Liquid PUC systems have limited applicability due to reasons relating to production and durability. Therefore, solid PUC materials would be advantageous.[11,22] Several approaches for developing solid-state PUC materials have been reported.[23] Many of these reported PUC materials can be categorized as semi-solid or rubbery where the (partly) soft nature of the material enables PUC governed by molecular diffusion.[24–30] Another approach for achieving solid-state PUC materials would be to replace the traditional *inter*molecular PUC system, where the interaction of the two types of upconversion molecules is governed by molecular diffusion, with an *intra*molecular system where the two molecules are combined into one entity. Such a molecular construct could potentially perform PUC without molecular diffusion and could hence be used in a solid-state PUC material.

1.3 Singlet Fission

Singlet fission is the opposite to TTA – it is the formation of two low energy excited states from one initial high energy excited state. The process of SF will be descried in more detail in Section 2.3 but can simplified be described as an electronic interaction between two molecules where the excitation energy initially localized on one of the molecules is split up and shared by both molecules in two independent excitons. In contrast to PUC, where the final product is an upconverted photon that can be absorbed by a solar energy device, the two excitons formed in SF are typically non-emissive. Utilization of SF for solar energy harvesting must therefore include an additional step, for example, electron injection into the charge separating layer of a solar cell,[31–35] or excitation energy transfer to an emissive compound that emits photons, which

subsequently can be absorbed by a solar energy device.[36–38] By implementing SF into photovoltaics, the theoretical upper energy conversion efficiency could be increased from ∼33%, as stated by the Shockley-Queisser limit, to ∼45%.[6]

SF was first observed in crystals of anthracene.[39] Because SF requires close contact between two chromophores, it was initially studied in crystals where each chromophore is always in close proximity to a neighboring chromophore within a well-defined structure.[40,41] It was not until 2013 that SF was observed for monomeric chromophores dissolved in a liquid solution.[42] Just as for TTA, SF can occur *intra*molecularly and the simplest system for *intra*molecular SF is a dimer with two connected chromophores.[43,44] As will be described in Section 2.3, the detailed mechanism of SF is not yet fully understood. Several studies of SF in dimers of chromophores have been published, where the intention has been to elucidate the detailed process of SF and the influence of the relative orientation of the two connected chromophores.[45–53] However, in many of these studies, the dimer molecule is assumed to be a single static entity defined by its molecular structure. By that assumption, dynamic effects such as conformational changes in the excited state are neglected and the distribution of different conformers present in a population of molecules is often simplified to only one lowest energy conformer. This motivates the investigation of *intra*molecular SF and the effect of molecular geometry that is presented in this thesis.

1.4 Research Questions

The long-term goal with both the PUC and SF research presented in this thesis is to develop new efficient molecular systems that can be utilized in solar energy technologies. For PUC, the strategy is to develop *intra*molecular PUC systems that could be implemented in a solid-state commercially viable upconversion material. For SF, the aim is so far to identify the key design parameters for achieving efficient *intra*molecular SF. The common denominator of the work presented in this thesis is thus the investigation of how a photophysical process that typically is governed by *inter*molecular interactions of individual chromophores diffusing in solution can be transformed into an *intra*molecular process, where the interacting chromophores are connected to each other. In the work presented in this thesis, well known PUC and SF chromophores have been used as model systems to gain insight into the electronic interactions between the chromophores. The overall research questions addressed in this thesis can be stated as follows:

- Is *intra*molecular PUC a versatile approach for developing solid-state upconversion materials?
- How does the *intra*molecular excitation energy transfer events function in an upconversion molecular framework, with respect to kinetics and efficiency?
- How does the relative geometry of the SF chromophores affect the rate of SF and the lifetime of the generated excitons?
- Are dynamic processes in the excited state useful for optimizing SF with respect to rate, efficiency and excited state lifetime of the generated excitons?

2

Theory

This chapter gives a brief introduction to the theory and photophysics that this thesis is based on. Light, matter, and their interactions are described from a perspective of optical spectroscopy with an emphasis on excitation energy transfer mechanisms. Finally, this chapter provides an overview of the photophysics behind PUC and SF.

2.1 Light and Matter

Light is the visible fraction of the continuous and infinite spectrum of electromagnetic radiation (EM radiation). EM radiation is a combined oscillating electric and magnetic field that propagates in a direction perpendicular to the direction of the electric and magnetic fields, as illustrated in Figure 2.1. EM radiation can be described both as a wave and a particle, a so called photon. The energy, E, of a photon is related to the wavelength, λ or frequency, ν, of the EM wave motion by Equation 2.1,

$$E = hc/\lambda = h\nu \tag{2.1}$$

where h is Planck´s constant and c is the speed of light. Visible light covers the wavelength range of approximately 400-750 nm, as illustrated in Figure 1.1. In optical spectroscopy, which the experimental methods used in this thesis are based upon, it is mainly the electric field of the EM radiation that is considered because the oscillating electric field can interact with the electrically charged electrons in atoms or molecules.

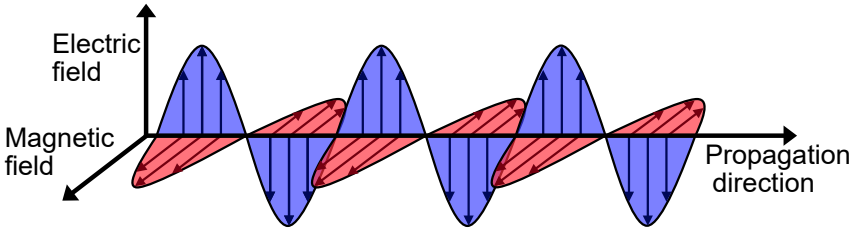

Figure 2.1: Illustration of EM radiation as an oscillating electric and magnetic field.

All objects and materials in the everyday world consist of atoms, which are built up by protons, neutrons and electrons. On a microscopic level, these particles are described by quantum physics. In contrast to objects in the macroscopic world, quantum systems are quantized in energy and exist in discrete states. An example of this is an atom or molecule in which the electrons are organized in discrete orbitals. For an electronic system, the states are given by the Schrödinger Equation, Equation 2.2.

$$\hat{H}\Psi = E\Psi \tag{2.2}$$

$\hat{H}$ is here the Hamiltonian operator describing the total energy of the system, Ψ is the wave function defining the state, and E is the energy of the state. The electronic wave function is related to the distribution of electrons as the probability of finding the electron in a certain volume in space (the probability density) is given by $|\Psi|^2$. Electrons are fermions and have spin of $+1/2$ or $-1/2$. Because electrons are fermions, they follow the Pauli exclusion principle, which states that two or more fermions can never occupy the same quantum state simultaneously. This has the consequence that each atom/molecule orbital can be occupied by maximum two electrons – one with spin $s = +1/2$ (spin up) and one with spin $s = -1/2$ (spin down). An important case to consider is a system with two electrons. The coupled spin of the two electrons can result in a net spin of $S = 1$ or $S = 0$, as given from the Clebsch-Gordan series.[54] If the net spin S is visualized as the magnitude of the coupled spin states, the direction of the net spin is defined by M_S, where $M_S = S, S-1, ..., -S$.[54] Hence, if the two electrons have antiparallel spin so that $S = 0$, there is only one possible state, which has $M_S = 0$. This is called a singlet state. If the two electrons have parallel spin, $S = 1$, there are three possible states with $M_S = 1$, 0 or -1. This is called a triplet state. The three triplet states are degenerate, that is they have the same energy, unless an external magnetic field is applied. In general, the multiplicity of a state is defined as $M = 2S + 1$, where M=1 is singlet state and M=3 is a triplet state. The two-electron system is important because the photophysical properties of atoms and molecules are mainly defined by the valence electrons in the frontier orbitals, the highest occupied molecular orbital (HOMO) and the lowest unoccupied molecular orbital (LUMO). For most molecules, the ground state has an electron configuration where each orbital up to the HOMO level is filled with two electrons of antiparallel spin, thus being a singlet. In the lowest energy electronic excited states, one electron is promoted to a higher lying orbital. Hence, there are two unpaired electrons which can have parallel or antiparallel spin, forming a triplet or singlet state, respectively, as illustrated in Figure 2.2. An exception to the rule of the ground state being a singlet is molecular oxygen, O_2, which is a triplet in its ground state.

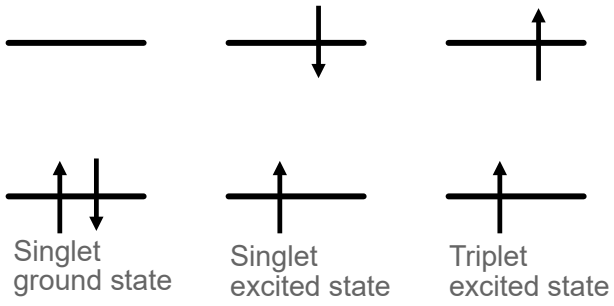

Figure 2.2: Schematic illustration of electron spin in states of singlet and triplet multiplicity.

Light and matter can interact and their interactions are the basis of photophysics and spectroscopy. The next sections will describe the absorption and emission of photons by molecules as well as the various relaxation processes and energy transfer events that can occur in the excited state.

2.1.1 Photoexcitation and Relaxation Processes

The oscillating electric field of EM radiation can interact with the electron cloud of an atom or molecule. EM radiation can add a perturbation that couples an initial state, for example a

molecule in the ground state, to a final state, a molecule in an electronic excited state, which leads to photoexcitation of the molecule by absorption of a photon. For a radiative transition to occur, where the transition between two states is induced by absorption or emission of a photon, the energy difference between the two states must equal the energy of the absorbed/emitted photon. This is called the Bohr frequency condition and is simply a criteria for energy conservation. The probability of a radiative transition is given by the transition dipole moment, and its magnitude is experimentally obtained from the intensity of absorption or the rate of emission. The oscillator strength is another measure of the transition probability. When a molecule absorbs a photon, it can undergo a variety of relaxation processes to return to the ground state. This is shown in a so-called Jablonski diagram in Figure 2.3. For each electronic state, illustrated as thick horizontal lines in the Jablonski diagram, there is a set of vibrational and rotational energy levels illustrated as a set of thinner lines. Photoexcitation typically occurs from the lowest energy level in the ground state to a higher vibrational level in the singlet excited state. From this state the molecule undergoes vibrational relaxation, dissipating the vibrational energy to surrounding molecules, in combination with internal conversion until the lowest energy level of the singlet excited state, S_1, is reached. The excited state lifetime of S_1 is typically much longer than the lifetime of higher excited states due to the usually large energy gap between S_1 and the ground state. From S_1, the molecule can return to the ground state by internal conversion and subsequent vibrational relaxation or by emitting a photon by fluorescence. Vibrational relaxation and internal conversion between excited states of the same multiplicity are usually very fast compared to other relaxation processes and therefore fluorescence typically occurs only from the lowest vibrational level of the S_1 state, as stated by Kasha´s rule. The molecule can also undergo intersystem crossing (ISC) to reach the triplet excited state, from which it can return to the ground state by ISC or emit a photon by phosphorescence.[55] Transition between states of different multiplicities are spin forbidden because it requires an electron to change spin. Therefore, ISC and phosphorescence are typically slow processes. However, the electron spin can couple to the electron orbital angular momentum, so called spin-orbit coupling, which makes the transition more allowed. The effect of spin-orbit coupling is stronger in molecules containing a heavy atom.

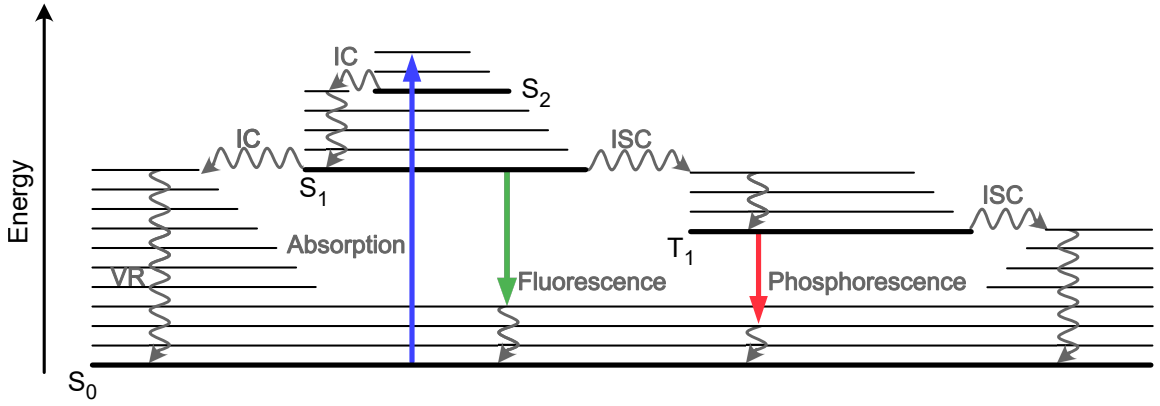

Figure 2.3: Jablonski diagram showing relaxation processes subsequent to photoexcitation by absorption of a photon, including vibrational relaxation (VR), internal conversion (IC), intersystem crossing (ISC), fluorescence and phosphorescence. S_0 denotes the singlet ground state and S_1 and S_2 the singlet excited states. T_1 denotes the triplet excited state.

The relative rate of the processes illustrated in the Jablonski diagram determines the quantum yield of the respective process. A quantum yield is defined as the number of quanta obtained (for example the number of emitted photons or excited states) per quanta of input (the number of absorbed photons). In the steady-state approximation, this can be rewritten as the relative rate of the process of interest to the combined rate of all competing processes. For example, the quantum yield of fluorescence, Φ_f, can be written as in Equation 2.3, where k_f is the rate of fluorescence and $\sum k_{nr}$ is the rate of all non-radiative decay processes.

$$\Phi_f = \frac{\#\text{emitted photons}}{\#\text{absorbed photons}} = \frac{k_f}{k_f + \sum k_{nr}} \tag{2.3}$$

As illustrated in the Jablonski diagram in Figure 2.3, the photons emitted by fluorescence or phosphorescence are typically of lower energy than the initially absorbed photon, as a result of vibrational relaxation. Another process that lowers the energy of the emitted photons is conformational relaxation. Radiative processes are vertical transitions, as illustrated in 2.4. This means that there is no change in atom position during the event of absorption or emission. Therefore, the conformation of the excited molecule will initially be the same as in the ground state. If the potential energy surface of the excited state has another shape or is shifted in position compared to the potential energy surface of the ground state, the molecule will undergo conformational relaxation to reach the new energy minimum conformation. This relaxation process gives rise to a shift in energy, called the Stokes shift, between the absorption and emission spectrum of a molecule, illustrated in Figure 2.4.

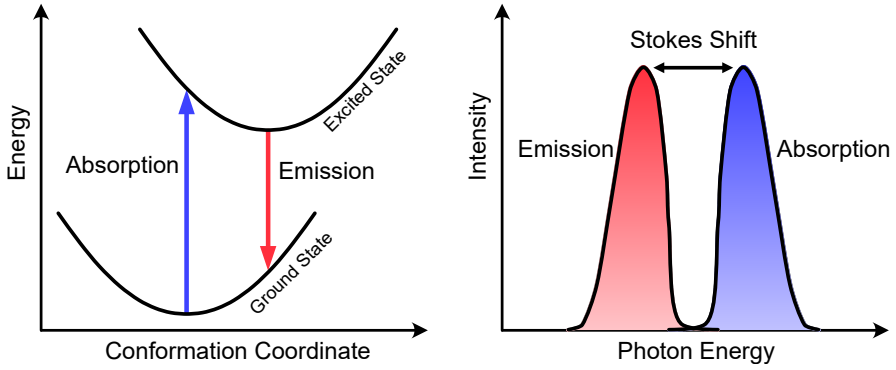

Figure 2.4: Left diagram shows potential energy surfaces of the ground state and excited state. Relaxation in the excited state leads to a Stokes shift between the absorption and emission spectrum, shown in the right diagram.

2.1.2 Excitation Energy transfer

Excitation energy can be transferred from a donor molecule in the excited state to another acceptor molecule in the ground state. There are two different mechanisms of excitation energy transfer: Förster resonance energy transfer (FRET) and Dexter energy transfer. FRET is governed by the coulombic dipole-dipole interaction, where the transition dipole moment of the donor couples to the transition dipole moment of the acceptor. The strength of the coulombic interaction is related to the radiative transition dipole moment of the donor and acceptor.[56,57] Thereby, the rate of FRET is related to the spectroscopically easily obtained parameters of fluorescence rate of the donor and absorptivity of the acceptor. In more detail, the rate constant of

FRET, k_{FRET}, is given by Equation 2.4,

$$k_{FRET} = \frac{R_0^6}{r_{DA}^6 \tau_D} \tag{2.4}$$

where r_{DA} is the distance between the donor and acceptor, τ_D is the emission lifetime of the donor in absence of the acceptor and R_0 is the so called Förster critical distance, given by Equation 2.5.

$$R_0 = 0.02108 \cdot \left(\frac{\kappa^2 \Phi_D}{n^4} J\right)^{1/6} \tag{2.5}$$

Φ_D is the emission quantum yield of the donor in absence of acceptor and n is the refractive index of the surrounding medium. κ^2 is a factor describing the orientation of the transition dipole moments of the donor and acceptor, as defined in Equation 2.6 and illustrated in Figure 2.5.

$$\kappa^2 = \left(cos(\theta_{DA}) - 3cos(\theta_D)cos(\theta_A)\right)^2 \tag{2.6}$$

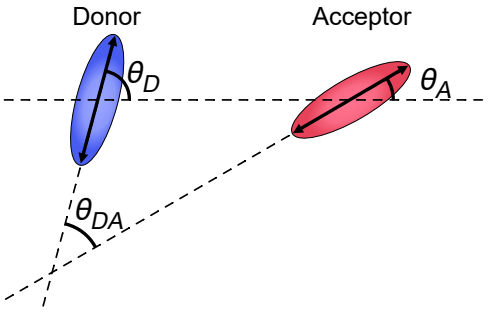

Figure 2.5: Illustration of the relative orientation of the transition dipole moments of the donor and acceptor.

J in Equation 2.5 is the spectral overlap integral (with the convenient unit $\text{mol}^{-1}\text{dm}^3\text{cm}^{-1}\text{nm}^4$ the way the equation is written here) between the donor emission spectrum and the acceptor absorption spectrum, defined in Equation 2.7, where $I(\lambda)$ is the area normalized emission spectrum of the donor, ε is the molar absorptivity of the acceptor and λ is the wavelength. An example visualizing the spectral overlap can be seen in Figure 4.6.

$$J = \int I(\lambda)\varepsilon(\lambda)\lambda^4 d\lambda \tag{2.7}$$

Equations 2.4-2.7 might seem hard to digest at first sight, but they can be understood from a more intuitive description: The rate of FRET depends on the coupling between the transition dipole moments of the donor and acceptor. The transition dipole moment of the donor is in these equations represented by τ_D together with Φ_D in Equation 2.4 and 2.5 respectively, while the transition dipole moment of the acceptor is represented by the integrated absorption spectrum in Equation 2.7. Further, the spectral overlap takes the energy conservation criteria of the overall process into account and the orientation factor κ^2 adjusts for the relative orientation of the transition dipole moments.

Dexter energy transfer is governed by the electron exchange interaction. Exchange interaction originates from the indistinguishability of electrons and has no classical analogue in the

macroscopic world. The rate constant of Dexter energy transfer decreases exponentially with increasing spatial separation of donor and acceptor, as described by Equation 2.8.

$$k_{Dexter} \propto e^{-\beta r_{DA}} \tag{2.8}$$

Even though the exchange interaction is a purely quantum mechanical phenomena, Dexter energy transfer can be visualized as a simultaneous exchange of electrons between the donor and acceptor, as illustrated in Figure 2.6. The attenuation factor, β, in Equation 2.8 is a measure of the height of the tunneling barrier for the exchange of electrons between the molecules. Dexter energy transfer requires that the electron orbitals of the donor and acceptor overlap spatially. This requirement is the origin of the exponential distance dependence in Equation 2.8, because the electron density typically decreases exponentially with distance from the atom nuclei. Further, the requirement of orbital overlap makes Dexter energy transfer a short-range mechanism (some few Å) that is often referred to as through-bond energy transfer. In comparison, FRET is described as a long range (a few nanometers), through-space mechanism with a simultaneous deexcitation and excitation of the donor and acceptor, respectively, as illustrated in Figure 2.6.

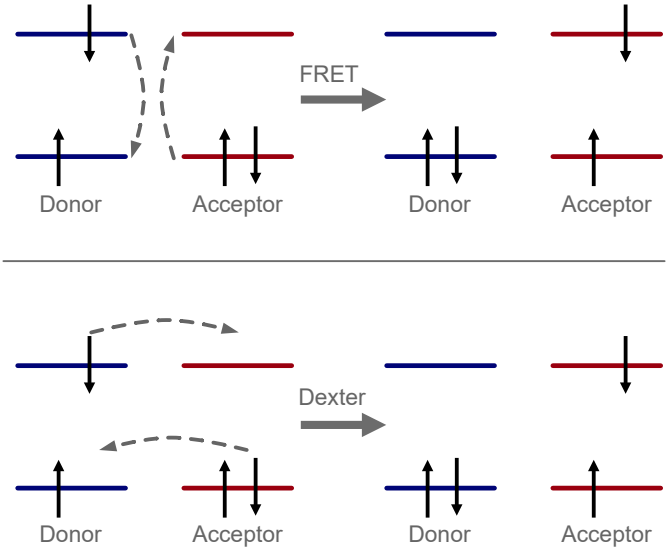

Figure 2.6: Schematic illustration of FRET (top) and Dexter energy transfer (bottom). Both processes are here illustrated with a donor in the singlet excited state, but can also occur with a donor in the triplet excited state.

2.2 Photon Upconversion

Photon upconversion involves two types of molecules: the sensitizer that absorbs the incoming low-energy photons, and the annihilator that emits the upconverted photon. The basics of the PUC process are illustrated in the Jablonski diagram in Figure 2.7. The sensitizer is photoexcited to the singlet excited state by absorbing an incoming low energy photon. It undergoes ISC to reach the triplet excited state. The excitation energy is transferred to an annihilator by triplet energy transfer (TET) where the sensitizer returns to the ground state and the annihilator reaches the triplet excited state. When two triplet excited annihilators interact, they combine their excitation energies by triplet-triplet annihilation (TTA) so that one annihilator returns to the ground state and the other is elevated to the higher lying singlet excited state. From the

singlet excited state, the upconverted photon is emitted by fluorescence. The sensitizer and annihilator molecules must fulfill some fundamental energetic requirements to enable PUC. First, the triplet energy level of the sensitizer must match the triplet energy level of the annihilator to enable TET. Second, the singlet excited state energy of the annihilator must not be higher than twice the energy of its triplet excited state. Further, to enable an overall efficient upconversion process, the sensitizer should have a high rate of ISC and the annihilator should have a high fluorescence quantum yield. Also the triplet excited state lifetime of sensitizer and annihilator is an important parameter, because a long-lived excited state increases the likelihood that the molecules can find a counterpart to undergo TET or TTA. This is especially important in liquid systems, as described below.

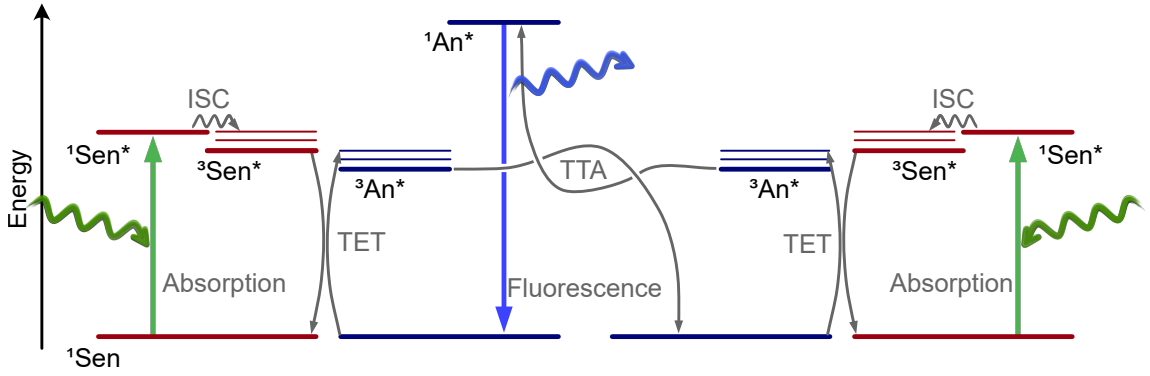

Figure 2.7: The process of photon upconversion, transforming two low energy photons (green curved arrows) to one higher energy photon (blue curved arrow), illustrated in a Jablonski diagram. The ground state and excited states of the sensitizer (Sen) and annihilator (An) are here shown in red and blue, respectively. The left superscript shows the spin multiplicity of the state and the asterisk indicates an excited state.

2.2.1 Quantum Yield and Efficiency

The quantum yield for the overall process of PUC, Φ_{PUC}, can be written as the product of the quantum yields of the substeps of ISC, TET, TTA and fluorescence, as written in Equation 2.9.

$$\Phi_{PUC} = f\Phi_{ISC}\Phi_{TET}\Phi_{TTA}\Phi_f \tag{2.9}$$

The maximum quantum yield of TTA, Φ_{TTA}, is $1/2$ (50%), because one excited state is formed from two initial excited states, and this sets the upper limit for Φ_{PUC}. Some researchers choose to present upconversion quantum yields normalized to a theoretical maximum of 100%. However, this way of presenting the yield of upconversion is better denoted as *normalized upconversion emission efficiency* and should not be confused with the actual quantum yield.[58,59] The factor f in Equation 2.9 is the spin statistical factor which describes the likelihood of generating a singlet excited state in the TTA event. Due to spin statistics, the combination of two triplets can result in singlet, triplet or quintet states with 1:3:5 relative ratio. In PUC, it is only the emissive singlet state that is desired and the other states of higher multiplicity are in that regard waste products. By that, only one out of nine TTA events could generate an upconverted photon and the maximum upconversion quantum yield would hence be $1/2 \times 1/9 = 5.6\%$.[60,61]

However, upconversion quantum yield up to around 40% have been reported, which is well above the spin statistical limit.[21] The breaking of the spin statistical limit can be explained from a closer look at the higher spin state and the spin statistics. First, the quintet is a high energy state with four unpaired electrons, which is typically energetically inaccessible. Second, when the combination of two triplets by TTA results in formation of one (high energy) triplet state, effectively only one exciton is lost because the resulting triplet can be reused in subsequent TTA events.[20,62] Further, it has been reported that the detailed spin statistics depends on the nature of the electronic coupling between the chromophores and their relative orientation.[63]

The upconversion quantum yield depends on the excitation intensity, as a result of the bimolecular nature of TTA. At low excitation intensities, the concentration of triplet excited annihilators is low and hence also the likelihood of TTA. The rate of TTA increases quadratically with the concentration of triplet excited annihilators, and thereby also with the excitation intensity.[64–66] At higher excitation intensities, the concentration of triplet excited annihilators can be high enough that essentially all of them can find an annihilation partner within their triplet lifetime. In this high excitation intensity regime, the rate of TTA, and thereby also the upconversion emission intensity, increases linearly with excitation intensity. The excitation intensity dependence of the upconversion emission intensity is often plotted in a double logarithmic plot, illustrated in Figure 2.8. The low and high excitation regimes can here be identified from the slope of the line fitted to the experimental data points. The slope is 2 and 1 in the low and high excitation intensity regimes, respectively. An excitation intensity threshold, I_{th}, can be obtained from the intersect of the two lines. The intensity threshold is defined as the excitation intensity at which half of the population of triplet excited annihilators undergo TTA under steady-state conditions.[64] The two regimes of excitation intensity are also seen in a plot of the upconversion quantum yield, which increases approximately linearly at low excitation intensity and reaches a plateau at higher intensities, as seen in Figure 2.8. The excitation intensity dependence is an important parameter to consider in the development of new efficient upconversion systems. In solar energy applications, the upconversion process must be efficient at the intensity of the solar light. Therefore, it is desirable that the I_{th} is well below the intensity of the solar light integrated over the sensitizer´s absorbance.

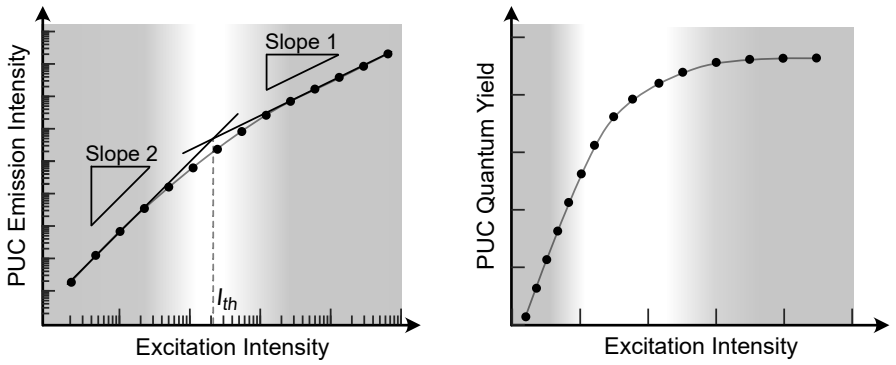

Figure 2.8: Schematic illustration of the excitation intensity dependence of PUC emission intensity in a double logarithmic plot (left) and quantum yield plotted in linear scale (right). The regions with quadratic and linear excitation intensity dependence are indicated by gray background shading. The intermediate region is shown with white background.

2.2.2 Inter- and Intramolecular Photon Upconversion

Both TET and TTA are examples of the Dexter type interaction and are spin allowed processes because the total spin momentum of the system is conserved. The whole upconversion process could therefore in theory be very fast. However, the most efficient upconversion systems are so far in liquid solution where the energy transfer events between the molecules occurs by *inter*molecular interactions in encounter complexes temporarily formed by Brownian motion. The whole process of *inter*molecular PUC is therefore governed and rate limited by the diffusion of molecules. With *inter*molecular PUC, the triplet excited state lifetime of the sensitizer and annihilator must be long enough so the molecules have time to find each other in the solution before spontaneously decaying to the ground state. When the molecules spend a long time in the excited state, they are susceptible to other quenching mechanisms such as triplet quenching by molecular oxygen. Therefore, PUC in liquids does not work under atmospheric conditions and must be properly deoxygenated to function, which is a great disadvantage for practical applications. As described in Chapter 1, *intra*molecular PUC would be advantageous as it enables PUC in solid-state materials. In an *intra*molecular PUC system, the sensitizers and annihilators could be connected to each other in a framework so that all energy transfer events would occur within the molecular construct governed by fast exciton migration, rather than molecular diffusion. A solid environment and an overall fast PUC process could make the upconversion insusceptible to oxygen. An *intra*molecular PUC system must be designed carefully. *Intra*molecular PUC requires the sensitizer and annihilator to be in close contact due to the short spatial range of the energy transfer events. However, connecting the sensitizers and annihilators to each other could result in additional quenching processes that are not present in a corresponding *inter*molecular system in solution, where the molecules on average are far from each other. In addition, the processes of TET and TTA are expected to be sensitive to the relative orientation of the chromophores due to the requirement of orbital overlap in Dexter type interactions. The orientation of the chromophores could have a major influence in *intra*molecular solid-state PUC where the molecules are locked in a defined geometry with limited conformational flexibility. In contrast, molecular orientation is not a prominent effect in *inter*molecular systems where the molecules interact in randomly formed conformations and have the possibility to reorient and experience multiple conformations in their attempts of TET or TTA.

2.3 Singlet Fission

Singlet fission is the formation of two triplet excited states from one initial singlet excited state, as illustrated in Figure 2.9. Because two excitons are formed from one initial, the maximum quantum yield of SF is 200%. The total process of triplet formation by SF can be divided into at least two substeps: first the formation of an exciton pair of correlated triplets with overall singlet multiplicity, ^{1}(TT), and subsequently exciton decorrelation into two independent triplet excitons. Just as for TTA, SF is a spin allowed process because the total spin momentum is conserved. The law of energy conservation puts a limit on the number of molecules that can undergo SF, as it requires the energy level of the triplet excited state of a SF chromophore to be equal to or lower than half the energy of its singlet excited state. Some examples of SF chromophores are diphenylisobenzofuran,[33,35,67] rylenediimides,[68–70] tetracene[40,71,72] and pentacene,[42,73–75] and derivatives thereof. The fundamental process of SF is not yet well un-

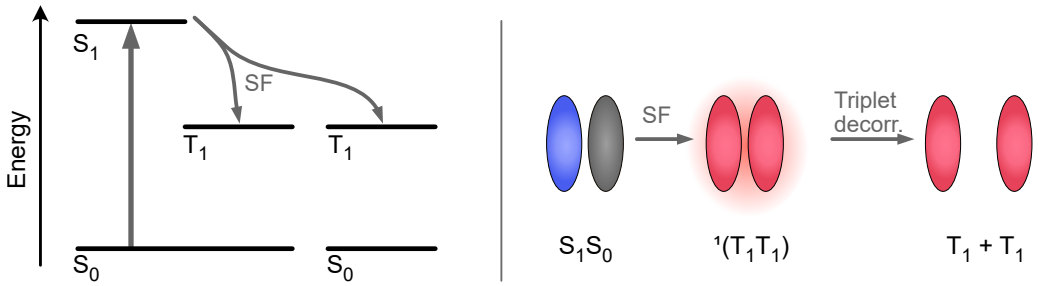

Figure 2.9: Left: Jablonski diagram of SF. Right: Illustration of triplet pair formation by SF and subsequent triplet decorrelation.

derstood and Figure 2.9 shows only a simplified picture. There is an ongoing discussion in the field about the detailed process and the influence of various intermediate states such as excimers, charge separated states and triplet pair states of overall quintet multiplicity.[63,76–87] The detailed process of SF and triplet decorrelation is best described as system dependent.

As mentioned in Chapter 1, SF can occur *intra*molecularly within a dimer with two connected chromophores. In a monomeric system in solution, the interaction of the chromophores is enabled by Brownian motion bringing the molecules together and *inter*molecular SF occurs in temporarily formed encounter complexes. In the same way, Brownian motion enables the formed triplet pair to become independent triplets by dissociating the excitons and spatially separating the molecules. In contrast, in *intra*molecular SF in a molecular dimer, the chromophores cannot dissociate, which limits the degree of decorrelation that can be achieved. Further, the excited state lifetime of the triplets formed by SF depends on the electronic coupling between the chromophores. Independent triplet excitons are generally long-lived, because the direct return to the singlet ground state is a spin forbidden process. However, in *intra*molecular SF, the formed correlated triplet pair is often short-lived because of the additional decay channel of triplet recombination that quenches the triplets before they are fully decorrelated. Long-lived triplet excitons is a requirement for efficient utilization of SF in for example solar energy technologies.

One parameter that has been identified to have a major influence on the process of SF and triplet decay is the relative orientation of the chromophores.[88–92] The conformation geometry of the dimer determines the magnitude of the through-bond and through-space electronic coupling between the chromophores, which determines the kinetics of SF and triplet decay. In a simplified picture, strong electronic coupling enables fast triplet pair formation by SF, but increases also the likelihood of triplet decay by triplet recombination.[93] This means that the design of molecular systems for *intra*molecular SF is a balance between strong enough electronic coupling between the chromophores to enable efficient triplet pair formation, but low enough coupling to enable formation of long-lived independent triplet excitons that can be harvested. The orientation of chromophores is of less importance when studying *inter*molecular SF in liquid systems where the chromophores interact in temporarily formed collision complexes and can do several attempts of SF in various geometries. However, in *intra*molecular SF, the chromophores are locked to each other in a more defined geometry. Hence, the study of *intra*molecular SF enables investigation of the effect of chromophore orientation and *intra*molecular electron coupling.

3
Methods

This chapter provides an overview of the methods used in this thesis. Experimental spectroscopic techniques are presented and various procedures for fitting experimental data to a physical model are described. Finally, it is briefly described how computational chemistry have been used in this thesis.

3.1 Steady-State Absorption and Emission

In steady-state absorption and emission spectroscopy, the radiative transitions between the electronic ground state and various excited states are investigated. By studying how the intensity of absorbed/emitted light depends on the wavelength of the light, information about the excited state energy levels can be acquired, according to Bohr´s frequency condition. Quantification of emission intensity can also provide information about decay channels from the excited state and energy transfer pathways.

3.1.1 Absorption Spectroscopy

UV-vis absorption spectroscopy can be used to identify the chromophores in a sample and measure their concentration. The optical outline of an absorption spectrometer can be seen in Figure 3.1. White light from a light source is passed through a monochromator. The monochromator usually consists of a diffraction grating, which split the incoming white light into different angles depending on wavelength, and a slit, which is used to select a narrow wavelength range to be passed towards the sample. The light is split up into two parallel beams: the probe beam and the reference beam. The probe beam is directed through the sample and onto a detector.

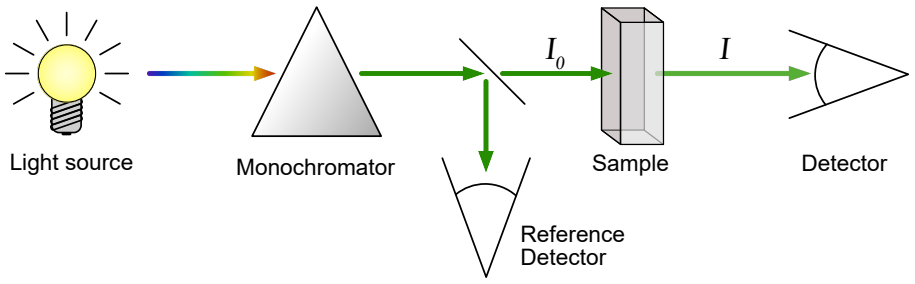

Figure 3.1: Schematic illustration of the optical setup of an absorption spectrometer.

The transmittance, T, of the sample can then be calculated from the ratio of the intensity of the light before and after the sample, I_0, and I, respectively, where I_0 is determined from the reference beam measured by a reference detector. Usually, the result is monitored as absorbance, A,

calculated according to Equation 3.1.

$$A = log_{10}(I_0/I) \tag{3.1}$$

By adjusting the monochromator, the absorbance of the sample at different wavelengths can be recorded and an absorption spectrum can be constructed. The absorbance of a sample at a wavelength, λ, is proportional to the concentration, C, of the dissolved solute according to Lambert-Beer´s law, Equation 3.2.

$$A(\lambda) = \varepsilon(\lambda)cl \tag{3.2}$$

Here, ε is the molar absorptivity, which is a measure of the probability of a molecule absorbing a photon of wavelength λ, and l is the optical path length through the sample (the sample thickness).

3.1.2 Emission Spectroscopy

An emission spectrometer generally consists of a light source, an excitation monochromator, an emission monochromator and a detector, as illustrated in Figure 3.2. Excitation light from a white light source is passed to the sample through the excitation monochromator, which is set to a wavelength that the sample absorbs. Light emitted from the sample is passed through the emission monochromator and directed towards the detector. By this design, an emission spectrum can be constructed from the recorded emission intensity at each wavelength set by the emission monochromator. Further, by scanning the excitation wavelength in the excitation monochromator while measuring the emission intensity at a fixed emission wavelength, an excitation spectrum can be constructed. The excitation spectrum will thus show which wavelengths of excitation light that give rise to emission and it does typically, but not necessarily, resemble the absorption spectrum of the sample.

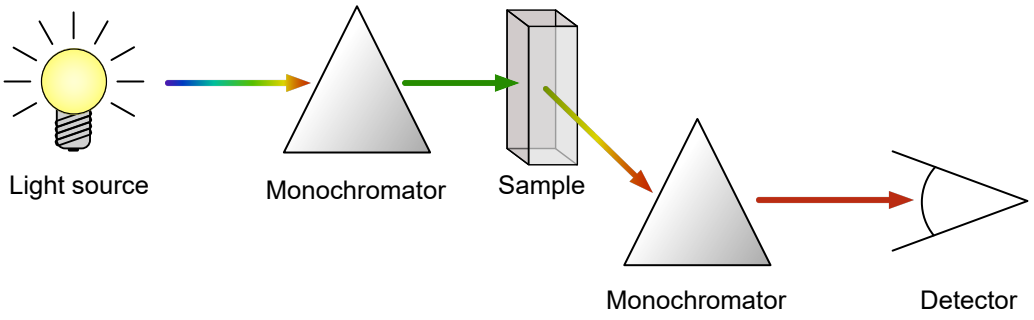

Figure 3.2: Schematic illustration of the optical setup of an emission spectrometer.

3.2 Transient Absorption

Transient absorption (TA) is a technique used to study the time evolution of an excited state by monitoring the absorption to higher lying states. Just like a steady-state absorption spectrum is a characteristic of the ground state and can be used to identify the chromophore components in a sample, the excited state absorption can be used to identify and track excited state species. TA is a pump-probe technique where the sample is first photoexcited using an intense light flash (pump) and the absorption spectrum of the sample is subsequently read out using a probe light, as illustrated in Figure 3.3. By varying the time delay between the pump and probe pulse,

a three-dimensional plot showing the time evolution of the TA spectrum can be constructed. Typically, the TA is plotted in a differential absorption spectrum, ΔA, as the absorption of the sample after pump pulse minus the absorption of the sample without pump pulse. Thanks to the logarithm quotient identity, ΔA at a specific wavelength and delay time can be calculated according to Equation 3.3

$$\Delta A = log_{10}(I_-/I_+) \tag{3.3}$$

where I_+ and I_- is the intensity of the probe light transmitted through the sample with and without a preceding pump pulse, respectively. By this, positive signals in the differential absorption spectrum will correspond to excited state absorption (ESA). ESA bands can sometimes be assigned to certain transitions and are then often denoted as $S_1 - S_n$ or $T_1 - T_n$ transitions, meaning a transition from the first excited state to one or several n:th higher excited states of singlet or triplet multiplicity, respectively. Depletion of the ground state population (ground state bleach) induced by the pump pulse together with stimulated emission induced by the probe pulse will result in a negative contribution to the differential absorption. Therefore, negative signals in the TA spectrum resembles the steady-state absorption spectrum superimposed with features from the emission spectrum, as illustrated in Figure 3.3.

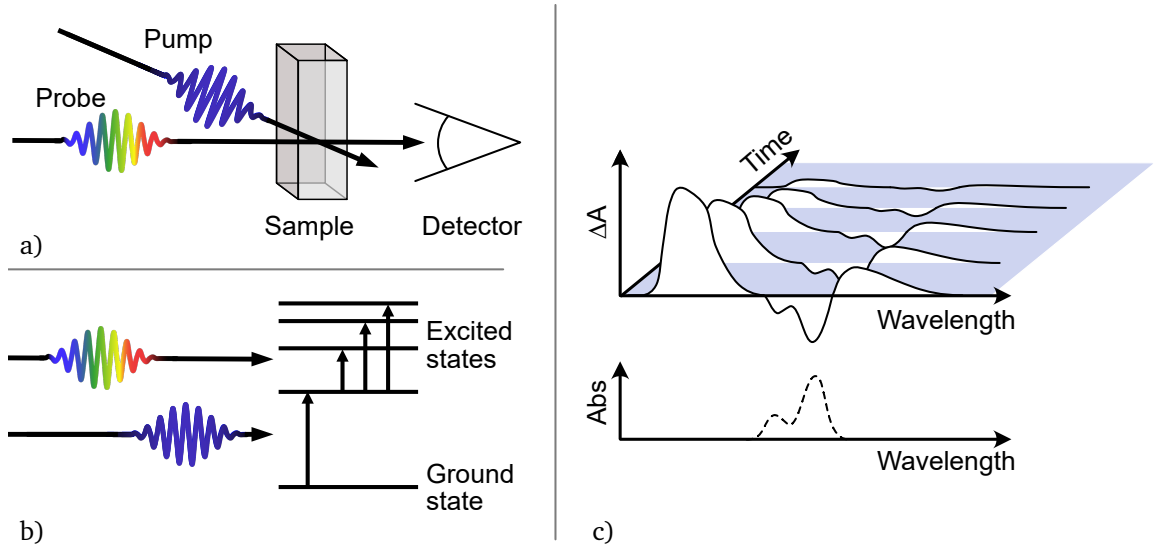

Figure 3.3: Schematic illustration of transient absorption. a) The sample is photoexcited with the pump pulse and the absorbance is measured using the subsequent probe beam. b) Excitation by pump pulse and probe pulse shown in a simplified Jablonski diagram. c) Transient absorption spectrum (upper graph) in comparison to steady-state absorption spectrum (lower graph).

The optical setup for measuring TA differs depending on the time resolution and the time window of interest. In nanosecond transient absorption (nsTA), monitoring photophysical processes in the time window of some few nanoseconds up to milliseconds, the time delay between the pump pulse and the read out of the probe can be controlled electronically. In the nanosecond TA setup used in this thesis, the pump pulse is generated by a nanosecond pulsed Q-switched laser. An optical parametric oscillator (OPO) is used to select the wavelength of the pump. The probe light from a continuous white lamp hits the sample in right angle to the pump beam and is directed towards the detector. A monochromator on the detection side of the sample enables monitoring of the TA signal in a narrow wavelength region. The TA signal is calculated from the variation in probe light intensity with time after the pump pulse. Depending on the

application, a photomultiplier tube (PMT) or photodiode can be used as detector for measuring the dynamics at a single wavelength. Alternatively, a charge coupled device (CCD) camera can be used to measure the time evolution of the full TA spectrum. In femtosecond transient absorption (fsTA), monitoring photophysical processes in the time window from some tens or hundreds of femtoseconds to some few nanoseconds, electronics is not fast enough so the delay between the pump and probe must be controlled optically. The setup used in this thesis is using a femtosecond pulsed laser (a mode locked Ti:sapphire laser with a regenerative amplifier) to generate both the pump and probe beam from the same laser pulse. The delay between the pump and probe is controlled by extending/contracting the optical path length of one of the beams in an optical delay stage. The probe beam is passed through a CaF_2 crystal to generate a white light continuum that is focused onto the sample, superimposed onto the focused pump beam. The transmitted probe light is passed to a CCD camera where the spectra with and without a preceding pump pulse are recorded. These spectra are then used to construct the three dimensional $\Delta A(\lambda, t)$ spectrum.

3.3 Time-Resolved Emission

Time-resolved emission spectroscopy can be used to monitor how the emission intensity or emission spectrum evolves in time after an excitation pulse. Depending on the time scale of interest, there are different techniques that can be used. At longer time scales, $> \sim$1 ns, modern electronics are fast enough to read out the transient signal directly from the emission detector, for example using a photodiode, a PMT, or a CCD detector. However, for measuring time-resolved emission at even shorter time scales, more advanced techniques are required. Two such techniques have been used in this thesis. The operation principle of these techniques are described below.

3.3.1 Time Correlated Single Photon Counting

The technique of time correlated single photon counting (TCSPC) is based on the measurement of the time after an excitation pulse that a photon emitted from the sample reaches the detector. A schematic illustration of the method is shown in Figure 3.4. The sample is excited with a pulsed laser where each laser pulse is shorter or similar to the time scale of the emission kinetics of interest. The emission from the sample is detected using a micro-channel plate photomultiplier tube (MCP-PMT) placed after an emission monochromator. Using various filters, the emission intensity detected by the MCP-PMT is turned down so that individual photons arriving at the detector can be resolved. By measuring the time of the first emitted photon arriving at the detector after an excitation pulse, and repeating over several excitation pulses, a histogram can be constructed with time after excitation on the x-axis and number of photons on the y-axis. This histogram represents the time evolution of the emission intensity. The time resolution of TCSPC is typically down to $\sim$50 ps, depending on the pulse width of the laser and the time response of the detector.

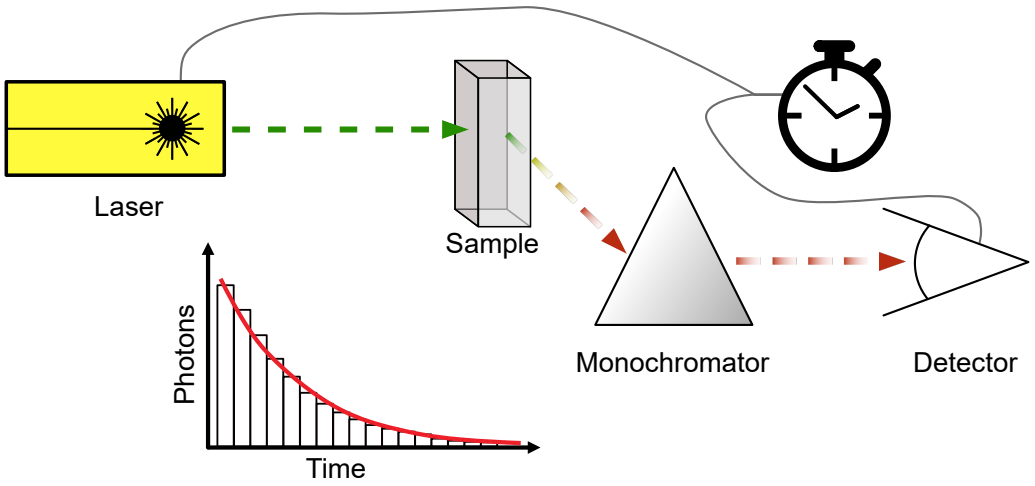

Figure 3.4: Schematic illustration of the operation principle of TCSPC.

3.3.2 Streak Camera Detection

Time resolved emission using streak camera detection enables a time resolution down to ∼1 ps or even shorter. A streak camera separates the emitted photons in different angles depending on both wavelength and on time of arrival. Streak camera detection can therefore show the time evolution of the whole emission spectrum, which is in contrast to TCSPC where the PMT detector only gives the emission time evolution at one wavelength set by the monochromator. The operation principle of a streak camera is shown schematically in Figure 3.5. The sample is excited using a pulsed laser. The photons emitted from the sample are directed into a spectrometer where they are separated in wavelength by a diffraction grating, causing them to propagate in different angles in one plane. A photocathode converts the stream of photons into a stream of electrons. Because electrons are electrically charged, they can be deflected by an electric field. By applying an increasing electric field, the electrons will be deflected according to time of arrival; the first arriving electron will experience a small electric field and only be slightly deflected, while later electrons will experience a larger electric field and hence be deflected more. The electric field is applied in a direction so that the plane of deflection is perpendicular to the plane of the diffracted photons. By that, the propagation direction of the electrons is a function of emission wavelength in one dimension and a function of time of arrival in the other dimension. A phosphor screen is used to convert the stream of electrons back to a stream of photons, which is detected by a CCD camera. The acquired image is a grayscale color map showing emission intensity as a function of both time and wavelength.

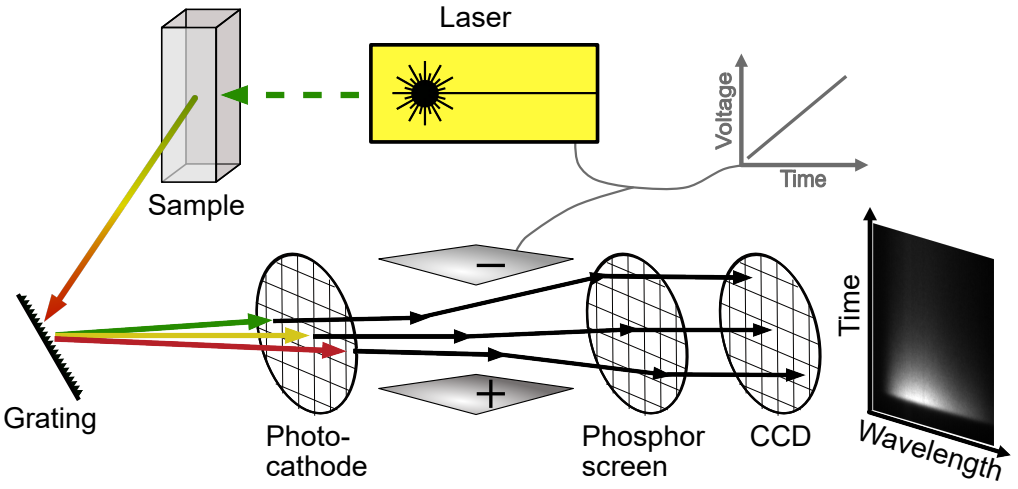

Figure 3.5: Schematic illustration of time resolved emission spectroscopy using streak camera detection.

3.4 Fitting Procedures

Extracting physical parameters such as rate constants or binding constants from experimental data requires a physical model that describes the system or the process. In this section, some fitting procedures and models used in this thesis are described.

3.4.1 Fluorescence and Phosphorescence – First-Order Kinetics

The rate constant of excited state deactivation can be extracted from the time profile of the emission decay signal following a short excitation pulse. Fluorescence and phosphorescence from an excited chromophore are both examples of first-order kinetic processes. The rate of depopulating the excited state after a short excitation pulse can be described with a single first-order differential equation with a starting condition (Equation 3.4).

$$\frac{d[X^*]}{dt} = -k_E \cdot [X^*], \qquad [X^*](t=0) = [X^*]_0 \tag{3.4}$$

Here, $[X^*]$ is the concentration of the excited chromophore X, k_E is the rate constant of excited state deactivation and t is the time. It should be noted that k_E is the sum of all first-order processes that depopulates the excited state, including for example fluorescence/phosphorescence, internal conversion and other non-radiative decay channels. The analytical solution to this differential equation is an exponential decay as presented in Equation 3.5, where $[X^*]_0$ is the initial concentration of excited chromophores at time zero.

$$[X^*](t) = [X^*]_0 \cdot e^{-k_E \cdot t} \tag{3.5}$$

Because the emission intensity, I, is proportional to the concentration of excited chromophores, the emission decay traces following a short excitation pulse (as typically used in time resolved emission spectroscopy) can be fitted to a single exponential decay, where k_E is the fitting parameter of interest. However, sometimes a single exponential decay is not enough to to fit the observed emission decay and more advanced models, like a multiexponential decay (Equation 3.6), can be used. The physical interpretation of a multiexponential emission decay is that

the sample contains multiple subpopulations of the emitting chromophore, where each subpopulation, n, is adding one exponential term to the emission decay function with its own rate constant.

$$I(t) = \sum_n I_{0,n} \cdot e^{-k_{E,n} \cdot t} \tag{3.6}$$

Using Equation 3.5 or 3.6 for fitting an observed emission decay assumes that the instrument response function (IRF), that is the overall time response of the instrument combining the pulse width of the excitation source and the response profile of the detection system, is fast compared to the time scale of the emission decay. However, if they are on the same time scale, the observed emission decay, I_{obs} will be a function of the 'true emission' time profile, I, convoluted with the IRF (Equation 3.7).[94]

$$I_{obs}(t) = \int_{-\infty}^{t} IRF(x) \cdot I(t-x)dx \tag{3.7}$$

In order to take the IRF into account, the fitting is made using deconvolution of the IRF. The fitted emission decay function $I(t)$ in Equation 3.7 is chosen after the physical model describing the system and can for example be a single- or multi-exponential decay, as in Equation 3.5 or 3.6. The IRF is usually recorded by measuring the time profile of scattered light from the excitation pulse.

3.4.2 Upconversion Emission – Second-Order Kinetics

The time evolution of upconverted emission provides valuable information about the upconversion process. It can be used to extract for example the rate constant of TTA and the triplet excited state lifetime of the annihilator, parameters that otherwise might be difficult to measure directly due to the optically dark nature of the annihilator triplet excited state. As described in Section 2.2, TTA is a bimolecular reaction and follows second-order kinetics, which means that the rate of depopulation of the triplet excited annihilator, $^3A^*$, is proportional to the square of its concentration. The total rate equation for depopulation of $^3A^*$ in photon upconversion is given in Equation 3.8.

$$\frac{d[^3A^*]}{dt} = -2k_{TTA} \cdot [^3A^*]^2 - k_T \cdot [^3A^*] \tag{3.8}$$

The terms on the right-hand side of the equation reflects the different decay channels; the first term corresponds to the second-order TTA process with rate constant k_{TTA} and the second term corresponds to first-order internal decay with rate constant k_T. The factor 2 is included in the first term to take into account that two triplet excited annihilators are consumed for each TTA event. The analytical solution to Equation 3.8 is given in Equation 3.9.[66,95]

$$[^3A^*](t) = [^3A^*]_{(t=0)} \cdot \frac{1-\beta}{e^{t \cdot k_T} - \beta} \tag{3.9}$$

Here, $[^3A^*]_{(t=0)}$ is the concentration of $^3A^*$ at time zero. β is a dimensionless parameter reflecting the initial relative rate of TTA and internal decay at time zero, as defined in Equation 3.10.

$$\beta = \frac{2k_{TTA} \cdot [^3A^*]_{(t=0)}}{k_T + 2k_{TTA} \cdot [^3A^*]_{(t=0)}} \tag{3.10}$$

Because of the bimolecular nature of TTA, the upconversion emission intensity, I_{UC}, is proportional to the square of the concentration of triplet excited annihilators. Therefore, the time

decay of upconversion emission, $I_{UC}(t)$, is described by Equation 3.11.

$$I_{UC}(t) \propto \left([^3A^*](t)\right)^2 = \left([^3A^*]_{(t=0)} \cdot \frac{1-\beta}{e^{t \cdot k_T} - \beta}\right)^2 \tag{3.11}$$

By fitting the observed decay of upconversion emission intensity after a short excitation pulse to Equation 3.11, the annihilator triplet lifetime (=$1/k_T$) can be extracted. Further, if $[^3A^*]_{(t=0)}$ can be estimated, k_{TTA} can be extracted from Equation 3.10. It should be noted, though, that this fitting requires that the initial condition $[^3A^*](t = 0) = [^3A^*]_{(t=0)}$ can be defined. Usually this is not the case because the triplet excited annihilator is not formed directly from the excitation pulse but is populated by TET from the photoexcited sensitizer. Therefore, a short excitation pulse results in a nonzero build-up time of $[^3A^*]$ and hence an initial rise of the upconversion emission signal before it starts to decay, as illustrated in Figure 3.6. However, if for example the triplet sensitization process can be assumed to be much faster than the TTA process, the later part of the upconversion emission decay can be fitted to Equation 3.11. As given from Equation 3.10 and 3.11, the curvature of the upconversion emission decay trace depends on both k_{TTA} and $[^3A^*]_{(t=0)}$, where the latter depends on the excitation intensity. For example, Equation 3.11 reduces to a single exponential decay in the limit of $\beta = 0$.

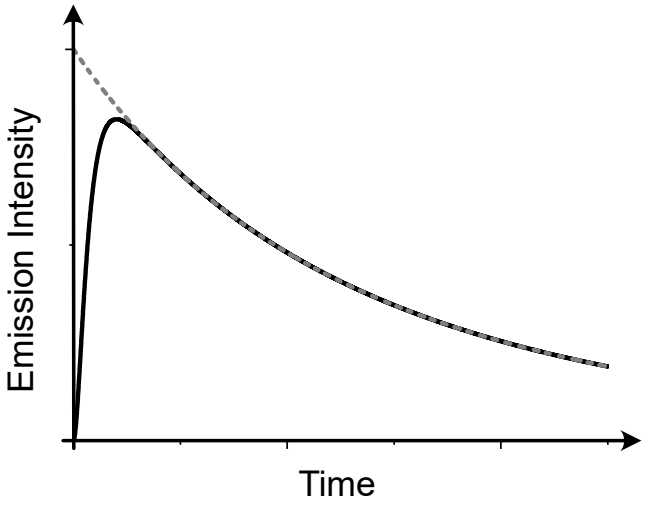

Figure 3.6: Illustration of the upconversion emission time profile. The black solid line shows the typical features of upconversion emission intensity after a short excitation pulse with a rise of the signal resulting from the population build-up of $^3A^*$ by TET from the photoexcited sensitizer and a subsequent decay of the signal. Gray dashed line shows fit of the decay profile to Equation 3.11.

3.4.3 Global Analysis and Singular Value Decomposition

The simplest form of data fitting is when the variation of one experimentally observed dependent variable is a function of one independent variable. This can for example be the variation in emission intensity at one wavelength over time. In spectroscopy, it is common that the dependent variable is a set of data, for example emission intensities at different wavelengths or a whole emission spectrum that varies with the independent variable, for example time. In such cases, global analysis can be used to extract the physical parameters in the model that are shared for the whole data set (global parameters) as well as the parameters that are unique for each data. In the example with an emission spectrum that decays with time, the emission life-

time could be a global parameter that is the same for all emission wavelengths. By using global fitting, the influence of measurement noise can be reduced because the fitting parameters that best fit the whole data set is calculated at once instead of for each individual data.

A method for global analysis that can be used to extract the individual spectral components in a set of spectra is singular value decomposition (SVD). SVD is based on linear algebra and is a generalized version of eigendecomposition for a non-square matrix.[96] It is a general mathematical tool that in this thesis has been used both to calculate the binding constant of a molecular complex from the absorption spectra in a titration series (Paper I) as well as for analyzing transient absorption data (Paper IV). Here, an example of time evolution of an absorption spectrum (transient absorption spectrum) will be used to describe global analysis by SVD.

An absorption spectrum or transient absorption spectrum is a linear combination of the individual spectra of each absorbing species in the sample (the spectral components). The experimentally obtained absorbance $A(\lambda, t)$ at wavelength λ and time t can be written as an $m \times n$ matrix,

$$\mathbf{A} = \begin{bmatrix} A_{1,1} & \dots & A_{1,n} \\ \vdots & \ddots & \vdots \\ A_{m,1} & \dots & A_{m,n} \end{bmatrix} \tag{3.12}$$

where each column represents a spectrum at a certain time and each row represents the time evolution of the absorbance at a certain wavelength. The SVD theorem states that an $m \times n$ matrix $\mathbf{A}$ can be decomposed into a product of matrices,

$$\mathbf{A} = \mathbf{U}\mathbf{\Sigma}\mathbf{V}^{\mathrm{T}} \tag{3.13}$$

where the columns of the $m \times m$ matrix $\mathbf{U}$ are orthogonal (linearly independent) spectral components spanning the spectral vector space of the spectra in $\mathbf{A}$. In the example of transient absorption, each spectral component represents one absorbing species. The $n \times n$ matrix $\mathbf{V}$ contains information about the intensity evolution profile corresponding to the orthogonal spectral components, that is, the concentration time profile of the respective species in the example of transient absorption. The elements of the diagonal $m \times n$ matrix $\mathbf{\Sigma}$ are the singular values corresponding to each spectral component in descending order where the magnitude of the singular values represents the weight of each spectral component. In a physical interpretation of the spectral decomposition, the number of spectral components necessary to describe the observed absorption spectra $\mathbf{A}$ should equal the number of absorbing species in the sample. However, $\mathbf{U}$ contains m spectral components, where m in the example of transient absorption equals the number of wavelengths in the spectra. Hence, only a few of the column vectors of $\mathbf{U}$ carries any significant spectral information. By reducing the matrices $\mathbf{U}$, $\mathbf{\Sigma}$ and $\mathbf{V}$ to $\mathbf{U_r}$, $\mathbf{\Sigma_r}$ and $\mathbf{V_r}$, only keeping the respective vectors corresponding to the significant spectral components, the measured absorption spectra can be approximated as in Equation 3.14

$$\mathbf{A} \approx \mathbf{A_r} = \mathbf{U_r}\mathbf{\Sigma_r}\mathbf{V_r^T} \tag{3.14}$$

Thereby the noise that is carried by the excluded spectral components can be reduced. There are multiple solutions to Equation 3.13 and the column vectors of $\mathbf{U}$ does therefore not necessarily resemble the real absorption spectra of the absorbing species in the sample. In order to find

the real absorption spectra as well as the corresponding concentration time profiles, a physical model describing the system must be defined. In the example with transient absorption, it is a kinetic model of how the absorbing species are related and how their concentrations evolve in time, which can be defined as a set of differential equations. This model is used to find the rotation matrix, $\mathbf{R}$ that best fits the observed spectra such that

$$\mathbf{V_r} = \mathbf{RC} \tag{3.15}$$

where $\mathbf{C}$ is a concentration matrix containing the concentration time profiles defined by the kinetic model. The fitted rotation matrix is then used to rotate the spectral component matrix $\mathbf{U_r}$ according to

$$\mathbf{T} = \mathbf{U_r R} \tag{3.16}$$

where $\mathbf{T}$ contains the absorption spectra of each species as defined in the kinetic model.[97] When SVD is used for analyzing transient absorption data, the obtained spectra in $\mathbf{T}$ are often referred to as species associated spectra (SAS).[98,99]

3.5 Computational Chemistry – Density Functional Theory

Computational chemistry has been used in this thesis as a complement to aid the discussion and interpretation of experimental results. More specificly, density functional theory (DFT) has been used to find the lowest energy conformation of various molecules and to calculate the potential energy of bending or rotation around a bond. Also, time-dependent DFT (TD-DFT) has been used to calculate electronic transitions of a molecule. Readers interested in the fundamental mathematics and quantum physics behind computational chemistry and DFT are referred to one of the several textbooks on the topic.[54,100] In this thesis, all DFT calculations were performed in the Gaussian 16 program package.[101]

Computational chemistry is basically about numerically solving the Schrödinger equation for an electronic system, Equation 2.2. The DFT method is based on the Hohenberg-Kohn theorem, stating that the total energy of the system can be determined from the electron density.[102] The energy is hence described as a functional (a function of a function) of the electron density, which is a function of space. The electron density in DFT is described as a linear combination of orbitals, which in turn are described as linear combinations of orthogonal functions in a basis set.[103] This can be seen as an analogy to a vector space where any vector (electron density function) in a space can be described as a linear combination of a set of orthogonal basis vectors (basis functions) spanning that space. Because it is impossible to use an infinite complete basis set, a truncated set is used where only the significant basis functions are present. Therefore, the choice of basis set in DFT calculations is important and must be done with care to balance between accuracy of the result and computational cost. Also the functional to use must be chosen with care depending on the molecule and property of interest, because different functionals take the electron exchange and correlation energy into account in different ways.

When searching for the lowest energy conformation of a molecule, the principle algorithm of a DFT calculation is as follows: A first start guess of the position of the atomic nuclei in the molecule of interest is made based on chemical intuition of what could be anticipated to be close to its lowest energy structure. Based on the given nuclei coordinates, an initial guess

is made on the electron density around the nuclei. From the electron density, the energy of the system can be calculated using the chosen functional. The electron density that gives the lowest energy for that particular molecular geometry is then found by iterating over the electron density in a self-consistent procedure. In a second outer iteration loop, the nuclei can be re-positioned and the energy of this new conformation is calculated as above. This procedure is repeated iteratively until convergence, which yields the minimum energy conformation of the molecule. The obtained lowest energy conformation of a molecule can be interesting in itself but can also be used as a starting point to investigate for example how much energy that is required to bend or rotate a molecule. This can be done by changing one coordinate (that is, an atom position, a bond length or bond angle) and calculating the energy of the new conformer in a single point calculation. However, only forcing the molecule to bend/rotate around one coordinate and calculating the energy of the new conformer does typically not yield a correct representation of the real system. This is because in a real molecule the other coordinates would adapt to the new bent/rotated structure and relax to find a new energy minimum. To take this into account, a relaxed scan can be performed where only one coordinate is locked and all other coordinates are free to optimize. An illustration of a relaxed versus non-relaxed scan is shown in Figure 3.7. A relaxed scan was used in Paper IV where the potential energy of rotation around a bond connecting two pentacene units was calculated, as will be described in Section 5. Finally, TD-DFT can be used to calculate properties of the excited state. For example, it can be used to calculate the electronic transitions of a molecule in a given molecular conformation. The energy of the electronic transitions together with their oscillator strength (intensity) can be used to construct an absorption spectrum of the molecule. This was done in Paper IV where the calculated electronic transitions of various conformers of the same molecule was compared to the measured absorption spectrum, see Section 5.

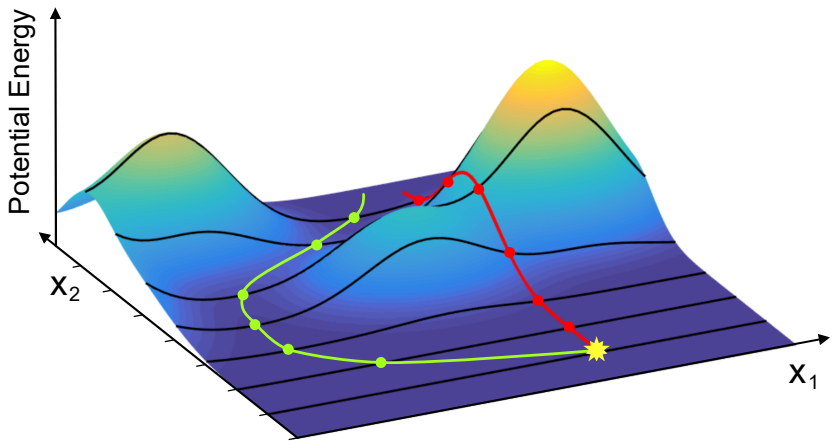

Figure 3.7: Illustration of relaxed and non-relaxed scan in a two-dimensional space, scanning over coordinate x_2, starting at the point marked by the yellow star. The green path illustrates a relaxed scan, where the system is free to relax in the other coordinate(s) for each each set position in x_2. The red path shows a non-relaxed scan where coordinate x_1 is kept fixed while scanning over coordinate x_2.

4

Intramolecular Photon Upconversion

This chapter presents the central results from Paper I-III,[104–106] describing the search for *intra*-molecular photon upconversion systems. The substeps in the upconversion process have been analyzed separately in a stepwise approach to gain insight in the parameters that are important for designing efficient *intra*molecular upconversion systems. In the first section, the energy transfer processes within a sensitizer-annihilator complex are described. This is followed by a section where *intra*molecular TTA in an annihilator polymer is studied. In all investigations presented in this thesis, the upconversion systems have been composed of a metal porphyrin as sensitizer and various derivatives of 9,10-diphenylanthracene (**DPA**) as annihilator. The absorption and emission spectrum for such a system is exemplified with platinum octaethylporphyrin (**PtOEP**) and **DPA** in Figure 4.1. This sensitizer and annihilator constitutes a green-to-blue upconversion system. The low energy photons are absorbed by the sensitizer around 530 nm and the upconverted photons are emitted by the annihilator in the wavelength range of ∼400-475 nm

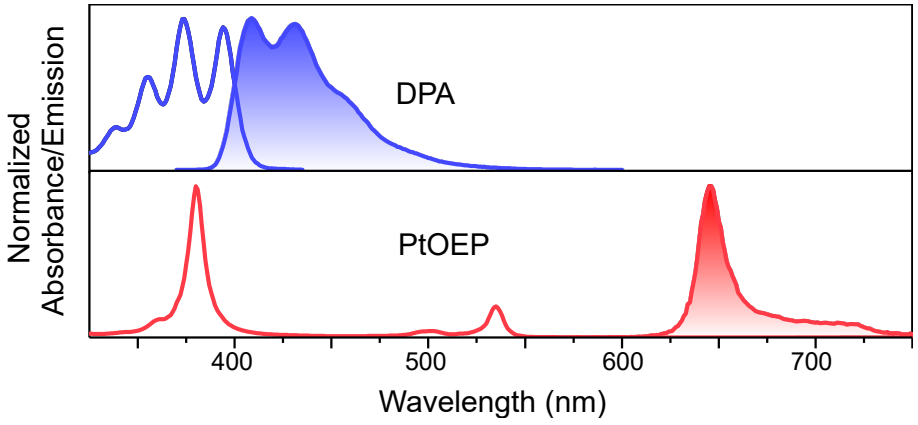

Figure 4.1: Absorption spectrum (unfilled) and emission spectrum (filled) of **DPA** and **PtOEP**

4.1 Sensitizer-Annihilator Interactions

To study the effect of attaching the sensitizer and annihilator to each other, a model system consisting of a sensitizer-annihilator coordination complex was investigated. A set of annihilator subunits was used in the investigation, seen in Figure 4.2. They all consist of a pyridine substituted derivative of DPA but have different features such as a varying number of phenylene spacers and anthracene moieties, which enables studying the effect of the sensitizer-annihilator spatial separation. For the sensitizer subunit, two different metal porphyrins were used: ruthenium(carbonyl) octaethylporphyrin (**RuOEP**) and zinc octaethylporphyrin (**ZnOEP**). The pyri-

dine substituent on the annihilator coordinates to the central metal atom in the porphyrin, forming a dative bonded Lewis acid-base-pair. The coordination geometry of the sensitizer-annihilator complex is defined by coordination cone angle, θ, between the annihilator ligand and the porphyrin plane, as schematically illustrated in Figure 4.2.

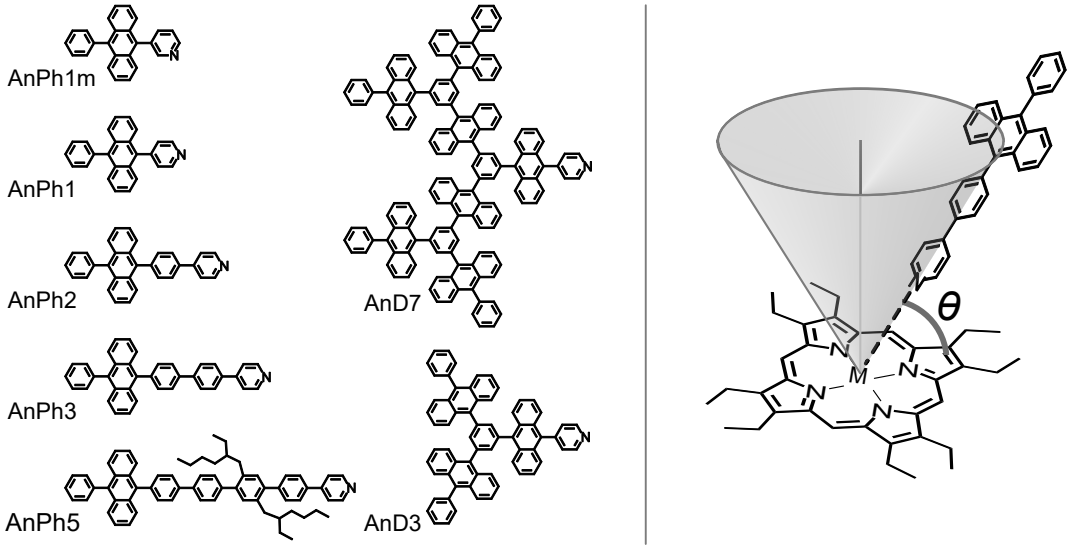

Figure 4.2: Left: The pyridine substituted anthracene annihilator subunits used in the study. Right: One example of the sensitizer-annihilator coordination complexes formed from an anthracene annihilator coordinating to a metal porphyrin sensitizer. M = Ru(CO) or Zn. θ is the coordination cone angle between the porphyrin plane and the coordinated annihilator ligand.

The sensitizer-annihilator binding constant have been determined using absorption titration. In this experiment, the change in the sensitizer absorption spectrum was followed as the concentration of the annihilator ligand was increased. The obtained absorption spectra were analyzed using SVD to extract the binding constant, as demonstrated in Figure 4.3.[104,107] The obtained binding constants varies a little for the different annihilator ligands but are in the range of 1-50$\times 10^6\,\mathrm{M}^{-1}$ and 2-6$\times 10^3\,\mathrm{M}^{-1}$ for **RuOEP** and **ZnOEP**, respectively. To illustrate what this difference in binding constant of the two porphyrins means, it can be calculated that in a solution of 100 μM with 1:1 molar ratio of sensitizer and annihilator, approximately 90% of the annihilator ligands will be coordinated to **RuOEP**, but with the same concentrations only approximately 30% will be coordinated to **ZnOEP**. More importantly, the different binding constants implies that the coordination lifetime of the complexes is different. The binding constant, K, is an equilibrium constant defined by the rate constant of complex formation of the complex, k_{on}, and the rate constant of dissociation, k_{off}, as described by Equation 4.1.

$$K = \frac{k_{on}}{k_{off}} \tag{4.1}$$

Assuming that the rate of formation is diffusion limited with $k_{on} \approx 10^9\,\mathrm{M}^{-1}\mathrm{s}^{-1}$, the rate constant of dissociation can be calculated as $k_{off} = k_{on}/K$. This calculation yields $k_{off} \approx 10^3\ \mathrm{s}^{-1}$ and $\approx 10^6\ \mathrm{s}^{-1}$ for the **RuOEP** and **ZnOEP** complexes, respectively. Hence, the coordination lifetime ($= 1/k_{off}$) is in the range of 1 ms for the **RuOEP** complexes but only $\sim$1 μs for the **ZnOEP** complexes.

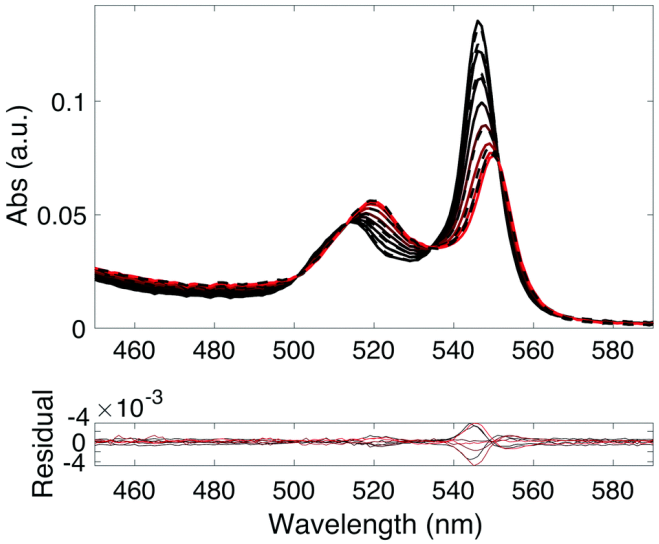

Figure 4.3: Shift in absorption spectrum of **RuOEP** upon ligand binding titration with **AnPh1m** as ligand, from black to red. Dashed lines show measured absorption spectra and solid lines show fitted spectra calculated using SVD. Reproduced from Ref. 104 with permission from the Royal Society of Chemistry.

4.1.1 Triplet Energy Transfer

The kinetics of triplet energy transfer in the sensitizer-annihilator complex was analyzed with **RuOEP** as the sensitizer using both ns-TA and time resolved emission spectroscopy. Photoexcitation of the **RuOEP** moiety results in almost quantitative ISC to its triplet excited state followed by TET to the coordinated annihilator. The annihilator triplet excited state is located only approximately 0.13 eV below the triplet excited state of **RuOEP**, therefore, thermally activated triplet energy transfer back to the sensitizer is possible (bTET).[104] This results in a pseudo-equilibrium between the triplet excited state of the **RuOEP** and the annihilator, as illustrated in Figure 4.4. The rate constants of TET, k_{TET}, and bTET, k_{bTET}, were obtained by studying the $T_1 - T_n$ transition of **RuOEP** in ns-TA. Due to the complex dynamics of excitation energy transfer in this system, the time profile of the **RuOEP** triplet excited state follows a biexponential decay where the two time constants contain information about k_{TET} and k_{bTET}.[108] The fitted time constants together with information about the intrinsic triplet lifetime of **RuOEP** and phosphorescence quantum yield of the complex could therefore be used to obtain k_{TET} and k_{bTET} for

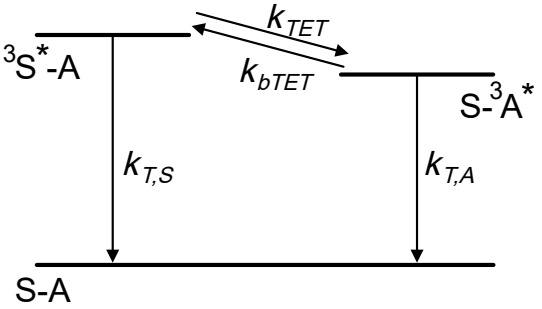

Figure 4.4: Jablonski diagram of the sensitizer-annihilator complex (S-A), showing TET and bTET between the triplet excited states of the **RuOEP** sensitizer and the coordinated anthracene annihilator. $k_{T,S}$ and $k_{T,A}$ are the rate constant of spontaneous triplet deactivation of the sensitizer and annihilator, respectively.

the different sensitizer-annihilator complexes, as presented in Table 4.1.

Table 4.1: Rate constants of triplet energy transfer (TET) and triplet energy back transfer (bTET) of the sensitizer-annihilator complexes with **RuOEP**. Data from Paper I.[104]

Ligand	k_{TET} (s^{-1})	k_{bTET} (s^{-1})
AnPh1m	$> 10 \times 10^9$	$> 2 \times 10^8$
AnPh1	3.6×10^7	7.3×10^5
AnPh2	7.6×10^5	2.1×10^4
AnPh3	8.4×10^4	1.7×10^3
AnPh5	3.3×10^4	0.2×10^3
AnD3	3.7×10^7	3.4×10^5
AnD7	3.8×10^7	2.4×10^5

As can be seen in Table 4.1, both k_{TET} and k_{bTET} decrease with increasing spatial separation of the sensitizer and annihilator (following the series **AnPh1**-**5**). This trend is expected considering that TET is a Dexter type process, for which the rate of energy transfer depends exponentially on the distance between the chromophores. That k_{bTET} is approximately two orders of magnitude lower than k_{TET} for these complexes reflects that bTET is an energetically uphill process owing to the energy separation of the sensitizer and annihilator triplet excited states. Comparing the meta coordinated annihilator, **AnPh1m**, with the para coordinated, **AnPh1**, it is clear that the rate constants of both TET and bTET is at least two orders of magnitude higher for the meta-coupled coordinated complex. This reflects the orbital overlap dependence of the Dexter energy transfer mechanism. Finally, for the two dendrimeric annihilators **AnD3** and **AnD7**, the rate constant of TET is very similar to that of **AnPh1**. This is expected considering that they are all coordinated to the **RuOEP** in the same geometry and with the same spatial separation between the sensitizer and the first anthracene moiety. However, the rate constant of bTET is lower for the larger dendrimeric annihilators. This could be caused by triplet exciton migration within the dendrimer, which results in an effective larger spatial separation of the annihilator triplet exciton and the sensitizer.

Taken together, the results presented here show that triplet sensitization of an annihilator is possible and can be very efficient in an *intra*molecular upconversion system. One drawback observed when connecting the sensitizer and annihilator is the triplet energy back transfer, but the effect of this could potentially be reduced by using a larger annihilator framework. It should also be noted that the investigation about bTET conducted for the **RuOEP** complexes could not have been performed in the same way for the **ZnOEP** complexes. This is because the coordination lifetime of the **ZnOEP** complex (as described above) is shorter than the expected rate constant of bTET, which means that the average **ZnOEP** complex will have time to dissociate before it has time to do bTET.

4.1.2 Singlet Energy Transfer

The previous section described the excitation energy transfer occurring on the triplet surface within a sensitizer-annihilator complex. Excitation energy transfer between chromophores can also occur between states of singlet multiplicity, so called singlet energy transfer (SET). For an

*intra*molecular upconversion system, the close proximity between the annihilator and sensitizer constitutes a risk of the fluorescence from the annihilator, that is the upconverted emission, is quenched by SET to the nearby sensitizer. In order to investigate the potential effect of SET in *intra*molecular upconversion, a set of sensitizer-annihilator complexes consisting of **ZnOEP** or **RuOEP** as sensitizer and **AnPh2**, **AnPh3** or **AnPh5** as annihilator was used (Figure 4.2). By photoexciting the annihilator moiety and studying the fluorescence decay kinetics, the rate constant of SET, k_{SET}, could be calculated for the different coordination complexes.

The calculated rate of SET as a function of the sensitizer-annihilator spatial separation can be seen in a double logarithmic plot in Figure 4.5. In comparison to the rate constant of annihilator fluorescence, which is approximately $2.5 \times 10^8\,\mathrm{s}^{-1}$,[107] k_{SET} is at least one order of magnitude higher for all complexes. This means that fluorescence from the anthracene moiety is outcompeted by SET to the coordinated porphyrin, and hence that any potential upconverted emission will be heavily quenched. It can also be noticed that k_{SET} is approximately one order of magnitude larger for the **RuOEP** complexes compared to the respective **ZnOEP** complex. In the following paragraphs, evidence will be presented showing that the mechanism of SET depends on the central metal atom in the porphyrin sensitizer; SET is governed by FRET in the **ZnOEP**-complexes but is governed mainly by Dexter energy transfer in the **RuOEP** complexes. Further, the FRET theory has been used to estimate the coordination angle between the porphyrin and anthracene moiety, which is discussed in relation to how SET quenching can be reduced in an *intra*molecular upconversion system.

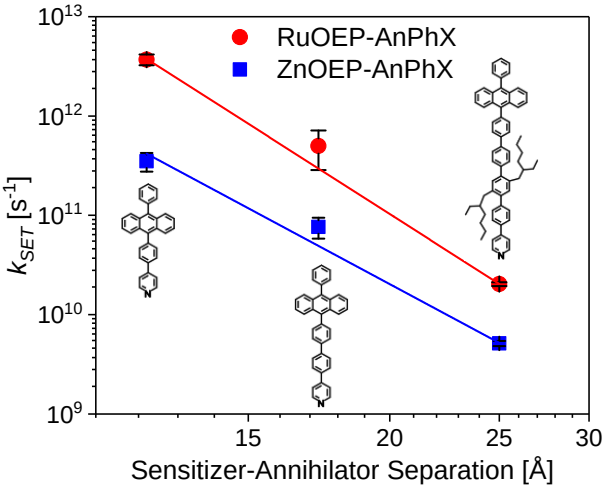

Figure 4.5: Rate constant of SET for the different sensitizer-annihilator complexes at room temperature. The sensitizer-annihilator spatial separation was estimated from the porphyrin central metal atom to the center of the anthracene core in an optimized structure.[107]

A first indication showing that different mechanisms are governing SET in the different complexes comes from the spectral overlap of the donor (anthracene) emission spectrum and acceptor (porphyrin) absorption spectrum, as seen in Figure 4.6. According to the FRET theory, Section 2.1.2, the rate constant of FRET is proportional to the spectral overlap. Hence, assuming a FRET based mechanism, the larger spectral overlap for the **ZnOEP** complexes should result in k_{SET} being higher for the **ZnOEP** complexes than for the **RuOEP** complexes, but Figure 4.5

shows the opposite. From this simple observation it is clear that the FRET theory cannot explain the observed SET in both the **ZnOEP** and **RuOEP** complexes.

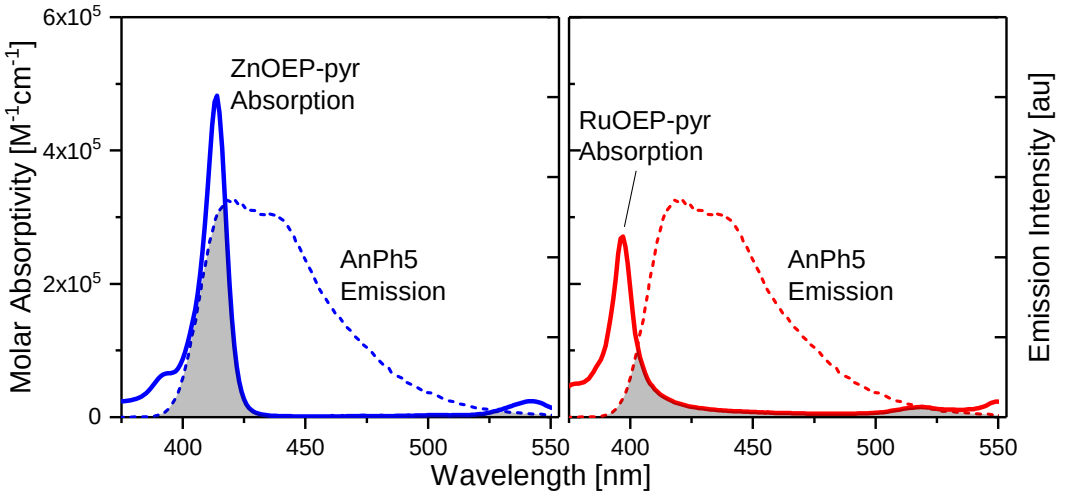

Figure 4.6: Illustration of the spectral overlap of the sensitizer-annihilator complexes with **ZnOEP** (left) and **RuOEP** (right) as sensitizer and **AnPh5** as annihilator. Absorption spectra of the pyridine coordinated porphyrin is here used to represent the absorption of the sensitizer moiety in the molecular complex. All spectra were measured at room temperature.

As described in Section 2.1.2, how the rate constant of SET depends on the distance between the donor and acceptor moiety can be used to elucidate the mechanism of SET. The distance dependence can be obtained from Figure 4.5, where the spatial separation of the donor (anthracene) and acceptor (porphyrin) is given by the length of the phenylene spacer bridge. The slope of the linear fit in Figure 4.5 is -6.11 $\pm$ 0.57 and -7.27 $\pm$ 0.18 for **ZnOEP** and **RuOEP**, respectively. This indicates that SET in the **ZnOEP** complexes is governed by FRET, for which a slope of -6 is expected (Equation 2.4). In contrast, the larger slope for the **RuOEP** complexes indicates that the FRET approximation is not sufficient to explain the observed rate of SET. Hence, the higher rate of SET for the **RuOEP** complexes must be a result of Dexter energy transfer in addition to FRET.

The total observed rate constant of SET for the **RuOEP** complexes can be described as a sum of Dexter energy transfer and FRET, Equation 4.2,

$$k_{SET} = k_{Dexter} + k_{FRET} \tag{4.2}$$

where k_{FRET} and k_{Dexter} are the rate constants of FRET and Dexter energy transfer component, respectively. It should be noted that this assumes that other quenching processes such as electron transfer can be excluded, which is further discussed in Paper II. The relative contribution of FRET and Dexter energy transfer in the **RuOEP** complexes can be estimated using the FRET theory. Assuming that both the **ZnOEP** and **RuOEP** complexes possess the same coordination geometry, that is, they have the same orientation factor, κ, and that SET in the **ZnOEP** complexes is governed only by FRET, the FRET component for the **RuOEP** complexes can be calculated from Equation 2.4 and 2.5, where the spectral overlap integral, J, is calculated from the measured absorption and emission spectra. The separated rate constant of FRET and Dexter

energy transfer is shown in Figure 4.7 for the **RuOEP-AnPh5** complex for various temperatures. k_{FRET} for **ZnOEP-AnPh5** is included in the same graph for comparison. As can be seen in this figure, the rate constant of Dexter energy transfer is dominating and contributes to 92-95% of the total observed SET at all temperatures.

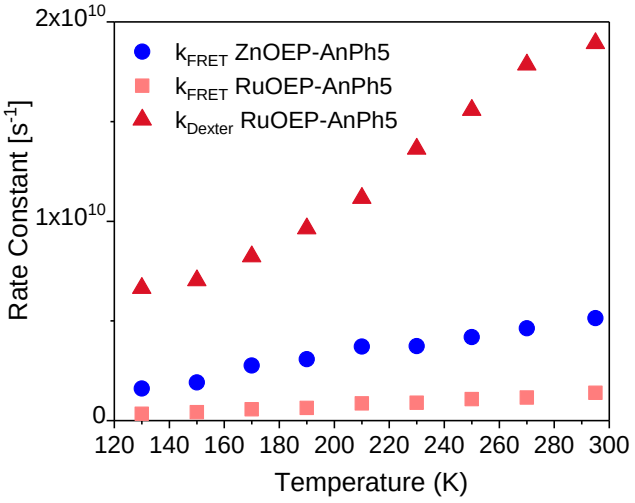

Figure 4.7: Rate constant of SET divided into its components of FRET and Dexter energy transfer for **RuOEP-AnPh5** and **ZnOEP-AnPh5** at various temperatures. Here, SET in **ZnOEP-AnPh5** is assumed to be governed solely by FRET, as concluded above.

The conclusion about FRET and Dexter energy transfer being the dominating mechanism of SET for the **ZnOEP** and **RuOEP** complexes, respectively, can be explained from a closer look at the molecular orbitals involved in the lowest energy transitions, shown in Figure 4.8. For **ZnOEP**, the molecular orbitals closest to HOMO and LUMO are centered on the porphyrin ring with negligible density on the Zn atom. Further, DFT calculations show that the lowest energy transitions in **ZnOEP** involves mainly the four orbitals shown in Figure 4.8. The lack of metal centered orbitals in the lowest energy transitions means that the through-bond electronic coupling between the porphyrin and the coordinated anthracene is weak, and hence the rate of Dexter energy transfer is low in the **ZnOEP** complexes and outcompeted by the through-space FRET mechanism. For **RuOEP**, the molecular orbitals contributing to the lowest energy transitions has a significant electron density on the Ru atom. For example, HOMO-4 can be described as an almost pure ruthenium 4d-orbital. The metal centered orbitals in **RuOEP** provides the necessary through-bond electronic coupling between the porphyrin and the coordinated anthracene that enables Dexter energy transfer to be the dominating mechanism of SET in the **RuOEP** complexes.

The investigation of SET in the sensitizer-annihilator complexes was intended to provide mechanistic insights in order to identify design parameters for reducing SET as a quenching process in *intra*molecular upconversion systems. One such design parameters is the coordination geometry of the complex; SET quenching by FRET should be eliminated if the anthracene moiety were coordinated perfectly perpendicular to the porphyrin plane, because in that conformation there is no overlap between the donor and acceptor transition dipole moment, yielding an orientation

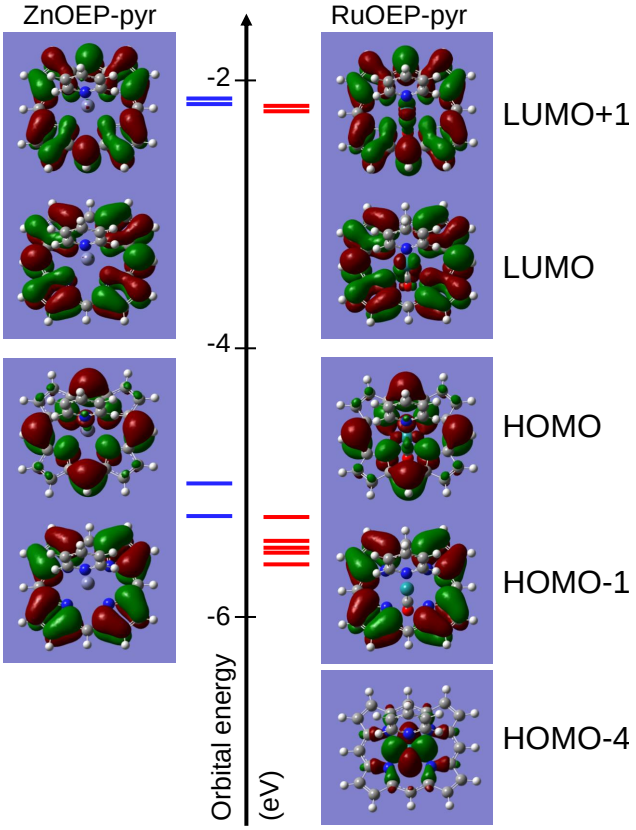

Figure 4.8: Frontier molecular orbitals of pyridine coordinated **ZnOEP** and **RuOEP**. Reprinted with permission from Ref. 105. Copyright 2019 American Chemical Society.

factor $\kappa = 0$. The perpendicular coordination, $\theta = 90°$, is the lowest energy conformation for the studied sensitizer-annihilator complexes and this is hence the coordination geometry that the complex would adapt at 0 K. However, at temperatures higher than 0 K, thermal energy enables the complex to adapt a tilted geometry, $\theta < 90°$, where the annihilator ligand can wiggle around in a cone, as illustrated in Figure 4.2. Therefore, the rate of FRET is expected to increase with increasing temperature, which in fact is observed in Figure 4.7. Further, the FRET theory can be used to estimate the effective coordination cone angle, θ. Using Equation 2.4 and 2.5, the orientation factor, κ^2, can be calculated from the measured rate constant of FRET. For the axially coordinated anthracene-porphyrin complexes it can be shown that κ^2 relates to θ as in Equation 4.3.[107,109]

$$\kappa^2 = 2cos^2\theta \tag{4.3}$$

Based on this relation it is found that θ varies from 76° at room temperature to 83° at 130 K for the **ZnOEP** complex with **AnPh5** as ligand.

Taken together, the results presented here show that SET quenching can be governed both by FRET and Dexter energy transfer. Which mechanism that dominates depends on the electronic coupling between the coordinated chromophores. FRET quenching could in theory be reduced by optimizing the geometry of the molecular complex. However, even though the studied sensitizer-annihilator complexes were designed so that the lowest energy conformation would inhibit FRET, molecular motion enabled by thermal energy distorts the molecular geome-

try enough to allow efficient FRET quenching of the annihilator fluorescence. Another approach for reducing SET quenching in *intra*molecular upconversion would be to use a large framework of annihilators coordinating to the sensitizer, thereby increasing the spatial separation of the annihilator singlet exciton and the sensitizer. Photon upconversion in a such annihilator framework is described in the next section.

4.2 Intramolecular Triplet-Triplet Annihilation

For designing a fully *intra*molecular upconversion system, each step in the upconversion process must be understood. The excitation energy transfer between the sensitizer and annihilator was analyzed in the previous section with respect to how the triplet sensitization dynamics works in a sensitizer-annihilator complex. In this section, *intra*molecular TTA (iTTA) in an annihilator polymer is analyzed with respect to kinetics and efficiency in comparison to a corresponding monomeric system.

For iTTA to occur, two or more annihilator units must be connected to each other in an annihilator cluster and at least two of the annihilator units in the cluster must get triplet sensitized within the triplet lifetime of the annihilator. The simplest annihilator system that enables iTTA is thus an annihilator dimer. Some few papers have been published where upconversion with annihilator dimers have been studied and some effects of iTTA have been noticed.[110–114] However, a challenge when studying iTTA in solution-based systems is the difficulty of spectroscopically separating the upconversion emission resulting from iTTA within one annihilator cluster from the upconversion emission resulting from *inter*molecular TTA (external TTA, xTTA) between two separate annihilator clusters. This difficulty has been the main limiting factor for making conclusions about the nature of iTTA. In the work presented in Paper III, an upconversion system with a polymeric annihilator was designed to enable isolation of iTTA. The annihilator framework in the studied system consisted of particles of an anthracene polymer dispersed in a solution. In this polymer, called triphenylbenzene-linked anthracene polymer (**TPBAP**, molecular structure seen in Figure 4.9), it is the anthracene moieties that constitute the annihilator units. Triplet sensitization of the annihilator is governed by diffusion mediated TET from the sensitizer platinum-octaethylporphyrin (**PtOEP**) dissolved in the solution surrounding the **TPBAP** particles. The triplet exciton can migrate within the **TPBAP** particle and once two triplet excitons are located in the same particle, they can undergo iTTA. In analogy with diffusion mediated upconversion, where (x)TTA usually denotes the combined process of molecular diffusion and subsequent TTA, iTTA is here considered as the process of triplet exciton migration within the annihilator particle and subsequent TTA. The comparably large size of the annihilator particles ($\sim$0.5 μm) results in very slow diffusion that prohibits diffusion mediated xTTA between two separate annihilator particles. To further reduce the probability of xTTA and increase the likelihood of double/multiple sensitization and iTTA, low annihilator concentration (5-30 μM, anthracene subunit concentration) was used in combination with high sensitizer concentration (1 mM). Figure 4.9 shows a schematic illustration of green to blue photon upconversion in the studied system with double sensitization and iTTA within the **TPBAP** particles.

The performance of the upconversion system with **TPBAP** was investigated using time resolved emission spectroscopy. Figure 4.10 shows the time traces of upconversion emission at various excitation intensities for the **TPBAP** system in comparison to an analogous reference system

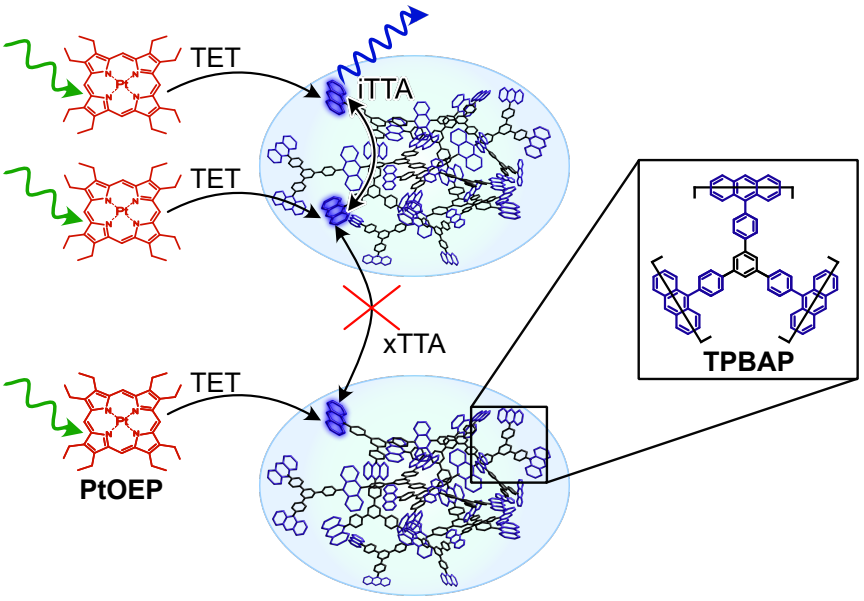

Figure 4.9: Schematics of photon upconversion with **PtOEP** and **TPBAP** as sensitizer and annihilator, respectively. iTTA within the **TPBAP** particles is enabled by double/multiple triplet sensitization and fast triplet migration within the TPBAP particle, while xTTA between between separate particles is prohibited due to slow diffusion of the **TPBAP** particles.

with monomeric **DPA** as annihilator. The upconversion emission time traces show an initial rise during the first few microseconds and subsequently a decay over some hundreds of microseconds. The rise time reflects the rate of annihilator triplet sensitization by diffusion mediated TET in combination with the rate of triplet migration/annihilator diffusion and TTA. As can be seen in Figure 4.10, the rise of the upconversion emission signal (upper panels) is significantly faster for the polymeric annihilator, even though the triplet sensitization process is the same in both systems. This is a clear indication that the upconversion is governed by iTTA in the **TPBAP** annihilator, where the process of triplet migration within the annihilator polymer is faster than the corresponding process of molecular diffusion and xTTA for the DPA annihilator. A further indication of upconversion governed by iTTA in the polymeric annihilator comes from the decay profile of the upconversion emission time traces at longer time scales, shown in logarithmic scale in the lower panels in Figure 4.10. As presented in Section 3.4.2, upconversion emission decay can be described by Equation 3.11. The curvature of an upconversion emission decay trace is given by the parameter β, as defined in Equation 3.10. $\beta = 0$ results in a single exponential decay, which is seen as a linear decay in a logarithmic plot, and $\beta = 1$ gives a faster non-exponential decay, seen as a curved decay in a logarithmic plot. Because β reflects the initial relative rate of triplet depopulation by TTA and by internal decay, it can be seen as a parameter describing the efficiency of TTA. As can be seen in Figure 4.10, the upconversion system with **TPBAP** shows a fast and non-exponential upconversion emission decay at the higher excitation intensities, indicating an efficient TTA process. This is in stark contrast to the upconversion sample with **DPA** which shows a single-exponential decay (seen as a straight line on the logarithmic scale), indicating that TTA contributes negligibly to the triplet depopulation. Because the excitation conditions and triplet sensitization process are identical for both

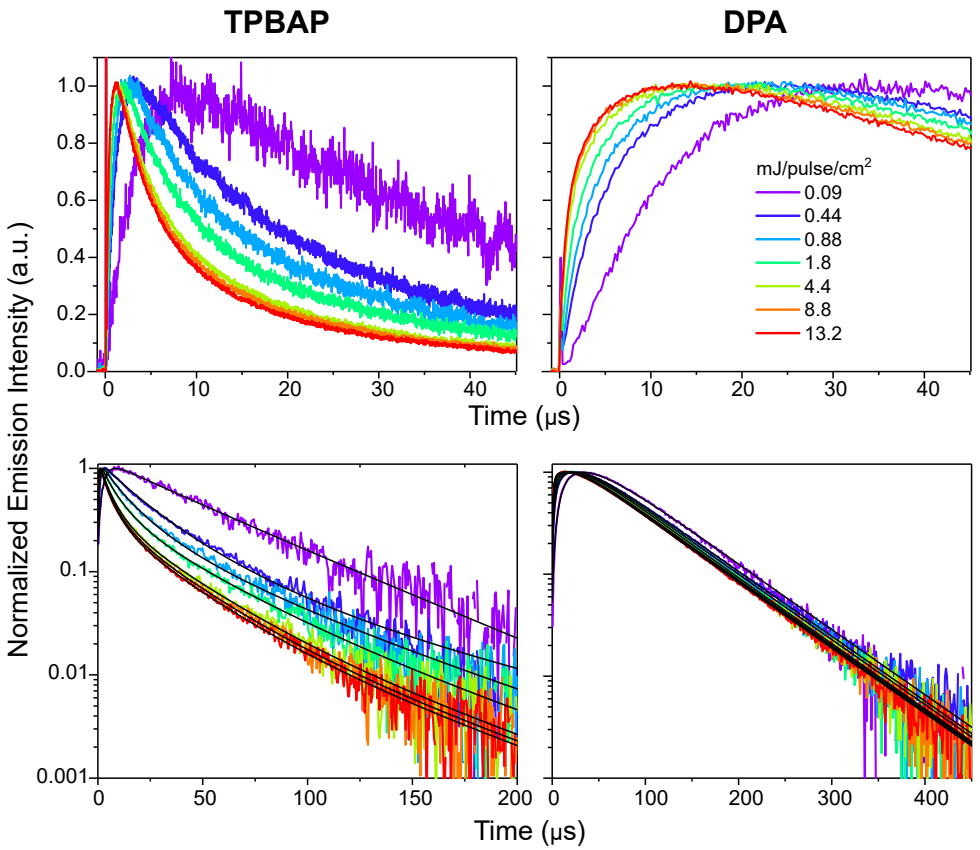

Figure 4.10: Time resolved upconversion emission at various excitation intensities with **TPBAP** (left) and **DPA** (right) as annihilator. Upper and lower panel shows the rise and decay of the upconversion emission signal at early and late time scales, respectively. Note the logarithmic scale on the y-axes in the lower panels. Also note the different timescales on the x-axes in the lower panels. Black lines in lower panels show fits to Equation 4.4. Annihilator subunit concentration 5 μM, **PtOEP** concentration 1 mM, excitation wavelength 532 nm, emission wavelength 440 nm.

the polymeric and monomeric upconversion system, this result can only be explained by iTTA with triplet exciton migration within the **TPBAP** particles being faster and more efficient than xTTA governed by molecular diffusion for **DPA**.

A value of β can be achieved by fitting the upconversion emission time traces in Figure 4.10 to Equation 4.4,

$$I_{UC}(t) = \left(g(t) + \alpha \cdot \frac{1-\beta}{e^{t \cdot k_T} - \beta}\right)^2 \tag{4.4}$$

which is a modified version of Equation 3.11 taking the rise of the upconversion signal into account. $g(t)$ is here included as an annihilator triplet exciton generation function and α is an arbitrary scaling factor representing the start concentration of triplet excited annihilator. From this fitting, a value of β can be achieved, which is plotted in Figure 4.11 for **TPBAP** and **DPA** as a function of excitation intensity. As expected from the curvature of the upconversion decay traces in Figure 4.10, the value of β for the polymeric upconversion system starts at a low value but increases with higher excitation intensity until it asymptotically approaches unity. In contrast, the value of β for the **DPA** upconversion system is low and close to zero for all used excitation intensities. The value of β is interesting in many regards as a figure of merit for the upconversion

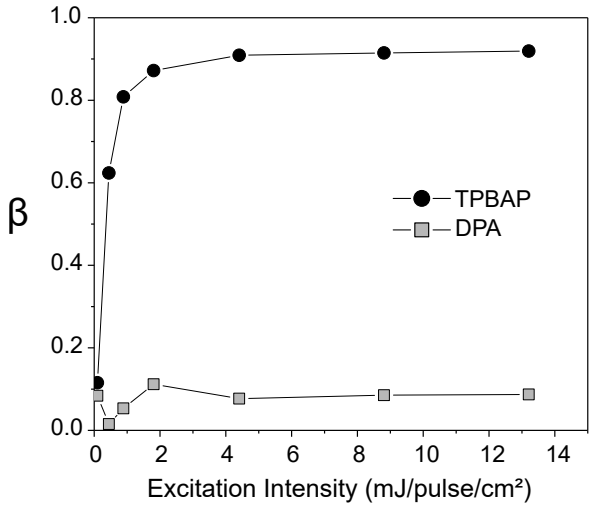

Figure 4.11: β as function of excitation intensity for **TPBAP** and **DPA**, 5μM annihilator subunit concentration.

system. First, β is a measure of the excitation intensity dependent efficiency of TTA under pulsed excitation. Therefore the excitation intensity at which $\beta = 0.5$ can be seen as pulsed excitation analogue to the upconversion intensity threshold, I_{th}, described in Section 2.2. With this definition it is clear from Figure 4.11 that I_{th} is much lower for the upconversion system with the polymeric annihilator **TPBAP** compared to its monomeric counterpart **DPA**. This can be explained by the fact that in the **TPBAP** annihilator, the annihilator triplet excitons are located in a confined space defined by the polymer particle, resulting in high local concentration of triplet excitons.[29,115] Hence, the likelihood of two triplet excitons to find each other and undergo TTA within their excited state lifetime will remain high even though the average number of annihilator triplet excitons in the whole sample is low. This enables a high rate of TTA also at low excitation intensities and hence a low I_{th}. However, at too low excitation intensity, the likelihood of achieving double/multiple sensitization of the annihilator particle is low resulting in a low β, which can be seen in Figure 4.11 as the fast drop in β for **TPBAP** at the lowest excitation intensities. Further, the fitted value of β can be used to calculate the rate constant of TTA, both for the iTTA within a **TPBAP** particle and for the xTTA between **DPA** molecules. Using Equation 3.10, the rate constant of xTTA for **DPA** was calculated to $k_{xTTA} = 9 \cdot 10^9\,\mathrm{M}^{-1}$, which is in the range of what would be expected for a diffusion controlled bimolecular process and similar to previously published values.[114] For **TPBAP**, k_{iTTA} was calculated to $1 \cdot 10^{12}\,\mathrm{M}^{-1}$, which is two orders of magnitude larger than the calculated k_{xTTA} for **DPA**. This shows that iTTA governed by triplet exciton migration in a polymeric annihilator framework can be a much faster than the corresponding process governed by molecular diffusion of a monomeric annihilator.

4.3 Summary of Intramolecular Photon Upconversion

In this chapter, the various electronic interactions between the chromophores in a sensitizer-annihilator complex have been investigated and *intra*molecular TTA within an annihilator polymer have been studied. This has been done in order to step by step analyze the versatility of *intra*molecular photon upconversion as a concept for developing solid-state upconversion materials. The presented results have shown that iTTA in an annihilator polymer particle can be very

efficient also at low excitation intensities because of fast triplet exciton migration and confinement of the triplet excitons within the annihilator particle. Even though the fully intramolecular system including also the sensitizer has not yet been tested, the study of the sensitizer-annihilator complex has shown that additional quenching pathways of excitation energy back transfer from annihilator to sensitizer may be activated when attaching the two chromophores to each other, both on the singlet and triplet surface. The influence of these quenching processes can be reduced by optimizing the electronic coupling between the sensitizer and annihilator. Further, exciton migration in a large annihilator framework can enable a larger average spatial separation of the annihilator triplet or singlet exciton and the quenching sensitizer. By that, *intra*molecular photon upconversion has potential as a concept for solid-state photon upconversion materials and solar energy applications.

5

Intramolecular Singlet Fission in Pentacene Dimers

This chapter presents the major findings from Paper IV. As described in Section 1.3, the detailed process of SF is not yet well understood. One of the key parameters affecting SF is the orientation of the two SF chromophores, which determines the electronic coupling between them. In paper IV, *intra*molecular SF was studied in a set of three pentacene dimers in order to elucidate the influence of chromophore orientation. The molecular structure of the dimers are shown in Figure 5.1. In all three dimers, the pentacene moieties are connected with a phenylene spaces bridge that enables rotation of the pentacenes relative each other. Various substituents on the phenylene unit add steric hindrance that result in different orientations of the pentacene units for the different molecules as well as a varying degree of rotational freedom. The rate of *intra*molecular SF and triplet depopulation in the pentacene dimers was investigated using fsTA. DFT calculations were used to aid the interpretation of the experimental results and to strengthen the conclusions thereof. A selection of the results for some of the pentacene dimers are shown here. The complete results and analysis is found in Paper IV.

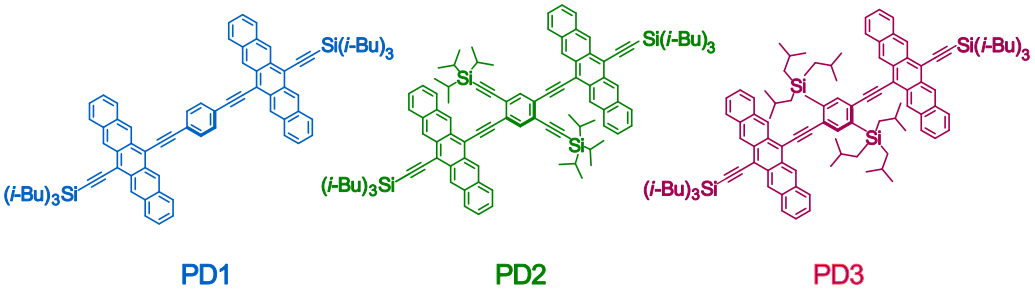

Figure 5.1: Molecular structure of the pentacene dimers **PD1-3**.

All three pentacene dimers undergo *intra*molecular SF upon photoexcitation, as can be concluded from the fsTA spectra in Figure 5.2. This conclusion comes from the assignment of the species associated spectra (SAS) extracted using SVD. An example of the obtained SAS can be seen in Figure 5.2b for **PD2**. The first spectral component, which has an excited state absorption (ESA) band centered at 450 nm, must be the singlet excited state because it is formed directly from the excitation pulse. This state is denoted S_1S_0 to indicate that one of the pentacene units is in its first singlet excited state and the other is in the singlet ground state. To assign the second component, its SAS was compared to the triplet nsTA spectrum of **PD2**, achieved from triplet sensitization by **PtOEP**, Figure 5.2c. From the clear overlap of the two spectra it can be concluded that the second spectral component must be a triplet excited state, or more specifi-

cally, it must be a triplet pair state, T_1T_1, formed by SF. All three dimers show similar SAS, as can be seen in Paper IV. The time scale of SF and triplet depopulation varies for the different dimers but are both in the order of 1-200 ps for all dimers. The fast triplet formation is a solid evidence that the process is governed by *intra*molecular SF, because any other triplet formation process such as *inter*molecular SF or ISC are expected to occur with a rate that is several orders of magnitude slower. The relatively short triplet excited state lifetime indicates that the formed triplet excitons are strongly correlated triplet pairs rather than free triplets.

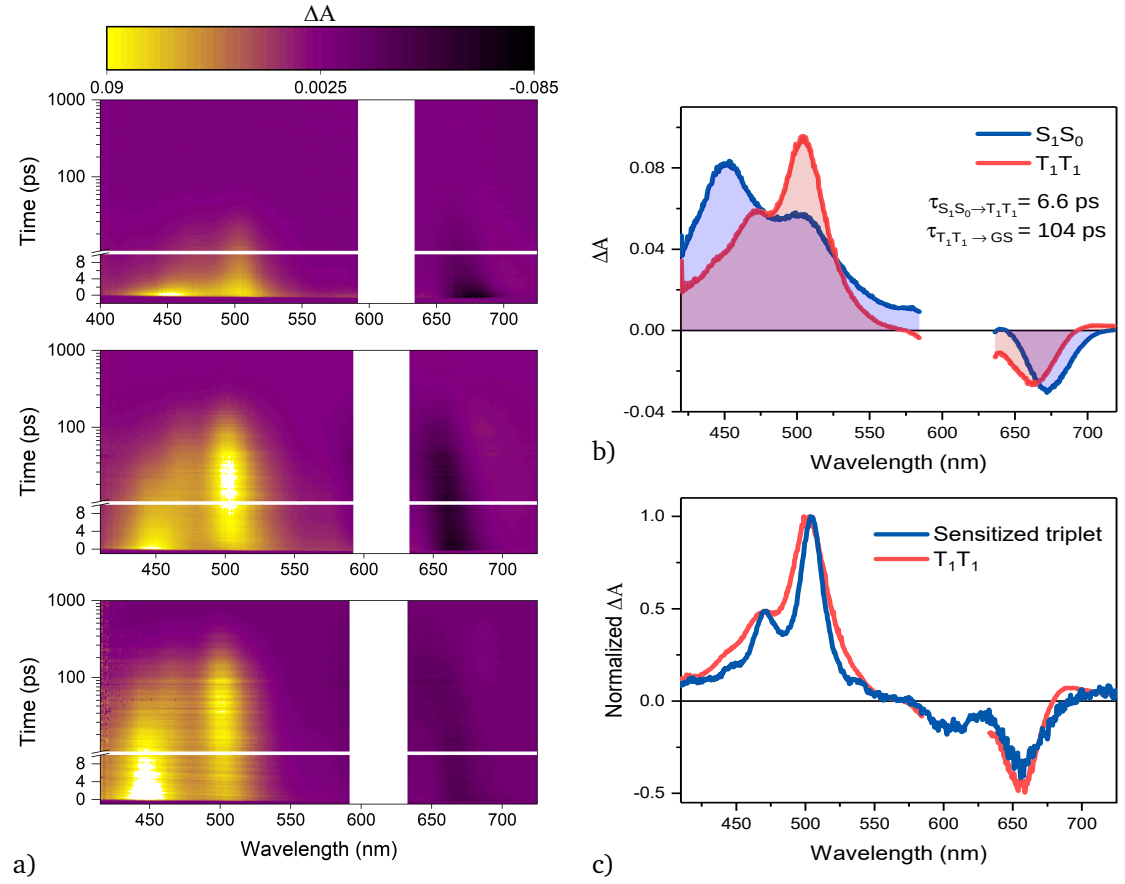

Figure 5.2: a) fsTA spectra of **PD1** (top), **PD2** (middle) and **PD3** (bottom) in toluene at room temperature with excitation wavelength 612 nm. b) SAS for **PD2** extracted using SVD assuming a two component kinetic model $S_1S_0 \rightarrow T_1T_1 \rightarrow$ ground state. c) Comparison of the SAS assigned to the T_1T_1 state for **PD2** with nsTA triplet spectrum of **PD2** achieved from triplet sensitization.

5.1 Effect of Rotational Conformation

The pentacene dimers can adapt various rotational conformations due to the rotational freedom around the bridge connecting the pentacene units. The geometry of the conformer that has the lowest energy results from conjugation and steric hindrance acting as counteracting forces that lowers and raises the potential energy, respectively. The lowest energy conformers of the pentacene dimers were calculated using DFT and are shown in Figure 5.3a. **PD1** adapts a planar structure where both the pentacene units and the pheylene spacer are coplanar as a result of maximum conjugation. The substituents on the phenylene spacer in **PD2** and **PD3** makes them adapt more twisted structures. For **PD2**, there is one global and one local minimum energy

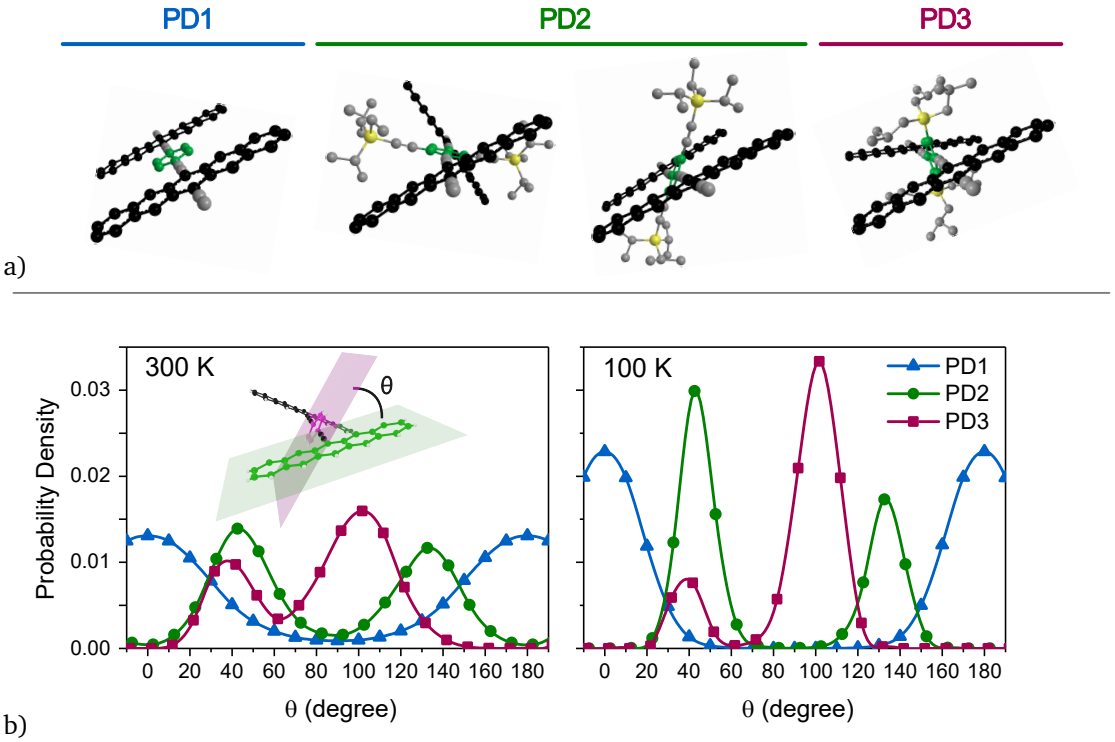

Figure 5.3: a) Lowest energy conformations of PD1, PD2 and PD3. b) Probability distribution of pentacene dimer rotational conformation at 300 K and 100 K, calculated using DFT in a relaxed scan with the basis set 6-31G(dp) and functional B3LYP. Inset figure illustrates θ as the dihedral angle between the plane of one of the pentacene units and the plane of the phenylene spacer. The lowest energy conformations in a) corresponds to the highest peak(s) in the respective probability distribution in b).

conformer at almost the same energy. The lowest energy conformations are the geometries that the molecule would adapt at 0 K, but other conformations will be present in a sample at higher temperature. These conformers must be considered when evaluating the effect of molecular conformation in *intra*molecular SF. The distribution of rotational conformers present in a population of molecules at thermal equilibrium is given by the Boltzmann distribution, Equation 5.1.

$$P(\theta, T) = \frac{e^{-V(\theta)/k_B T}}{\int e^{-V(\theta)/k_B T} d\theta} \tag{5.1}$$

P is here the probability density of finding a molecule in a geometry defined by θ at temperature T and V is the potential energy of the conformer. To estimate the potential energy of various rotational conformers, $V(\theta)$ was calculated using DFT in a relaxed scan (see Section 3.5). θ was here defined as the dihedral angle between the plane of one of the pentacene units and the plane of the phenylene spacer, as illustrated in Figure 5.3b. The rotational conformation probability distributions for **PD1-3** at 300 K and 100 K for θ=0-180° are shown in Figure 5.3b. Virtually all conformers across the range of θ are present at 300 K, but at 100 K, the distributions are much more narrow with larger weight on the lowest energy conformers. All rotational conformers have a varying degree of electronic coupling between the pentacene units, both by through-bond and through-space coupling, which influences the SF dynamics. To be able to study the SF kinetics for the various rotational conformers individually, they must somehow be separated. It is not possible to physically separate the different conformers, but they can

be distinguished spectroscopically by means of selective photoexcitation by choice of excitation wavelength.

The rotational conformers of a pentacene dimer can be seen as different absorbing species where the varying degree of electronic coupling give rise to slightly different absorption spectra. How much the absorption spectra differs for the various conformers was estimated from the lowest energy singlet transitions calculated using TD-DFT, as presented in Figure 5.4a. A comparison with the room temperature absorption spectrum of **PD1** is shown in the lower panel. The conformers used in these calculations are illustrated in the inset and were chosen to represent the lowest energy conformers seen in Figure 5.3. The lowest energy singlet electronic transition varies by ∼0.2 eV depending on conformer, which corresponds to approximately a variation of ∼50 nm in this energy range. This result indicates that different conformers could be photoexcited selectively. However, the broad range of rotational conformers present at room temperature shown in Figure 5.3 results in broad absorption bands for the dimers, as seen in Figure 5.4b, and it can be anticipated that the individual bands from the different conformers are underresolved and overlapped with the vibronic progression of other bands. At lower temperature, the distribution of conformers is narrower, which result in narrower and more resolved absorption bands, which is especially seen for **PD3** at 100 K, Figure 5.4b. By this, it can be assumed that excitation of various conformers can be more selective at low temperature. Hence, the fsTA measurements performed to elucidate the conformation dependence in SF were performed at 100 K.

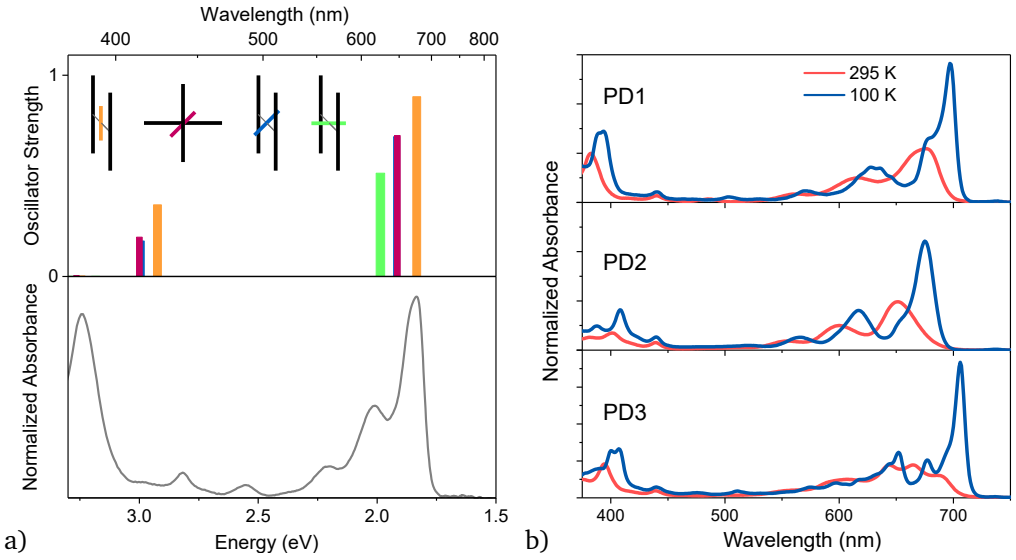

Figure 5.4: a) Lowest energy electronic transitions for a pentacene dimer in various conformations representing the lowest energy conformers of the three pentacene dimers. The calculations were done with **PD1** as a model compound in various geometries, using TD-DFT with the basis set 6-31G(dp) and functional CAM-B3LYP. The inset illustrates the geometry of pentacene dimer conformers with the pentacene units and the phenylene spacer pictured as black and colored bars, respectively. Note that the electronic transition of the red and blue conformers are similar in energy and oscillator strength and therefore overlaps in the diagram. Lower panel shows room temperature steady-state absorption spectrum of **PD1** in MTHF for comparison. b) Steady-state absorption spectra of **PD1-3** in MTHF at 295 K and 100 K.

The rate of SF and triplet depopulation at 100 K varies dramatically depending on excitation wavelength for all three pentacene dimers. An example of the excitation wavelength dependence can be seen in Figure 5.5 for **PD3**, for which this effect was most pronounced. The figure shows the time evolution of the fsTA signal at 505 nm, which corresponds to the ESA of the T_1T_1 state. Photoexcitation in the lowest energy absorption band at 707 nm results in triplet formation by SF faster than the time response of the instrument, ∼300 fs, and only the fast decay of the T_1T_1 state is seen with a time constant of 1.8 ps. This fast SF and triplet depopulation process implies a strong electronic coupling between the pentacene units in the conformer photoexcited by 707 nm. Changing the excitation wavelength to 651 nm, other conformers are excited, which results in more complex kinetics. Initially, there is an underresolved rise of the TA signal and a corresponding decay with a time constant of 1.6 ps, which is similar to kinetics obtained with excitation wavelength 707 nm. On longer time scales, there is a clearly resolved triplet pair formation by SF with a rise time constant of 153 ps. The formed triplet pair is comparably long-lived and decays with a time constant of 21 ns. This result with dual rise and decay of the T_1T_1 state indicates that two subpopulations of conformers have overlapping absorption spectra at the excitation wavelength 651 nm. The short-lived species is assigned to the same conformer that was selectively photoexcited using 707 nm and the longer lived species is assigned to a conformer with weaker electronic coupling between the pentacene units.

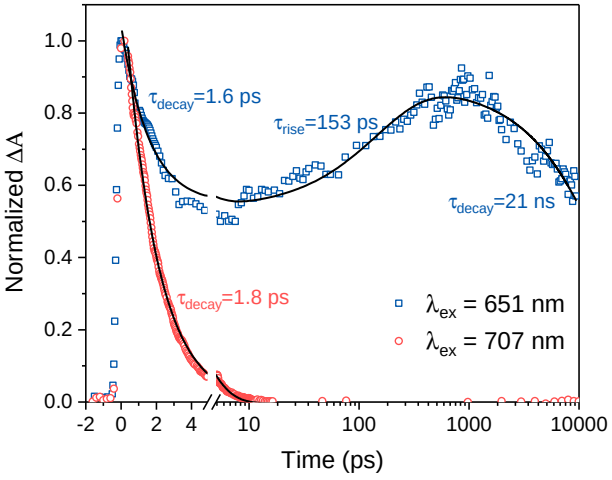

Figure 5.5: Time evolution of the fsTA signal at the 505 nm ESA band, corresponding to the T_1T_1 state, for **PD3**. Measured in MTHF at 100 K with two different excitation wavelengths. Black lines show fit to a sum of exponentials, $\Delta A = \sum_i a_i e^{-t/\tau_i}$ and the obtained time constants, τ, are shown in the graph.

Exactly which conformers that are photoexcited with the different excitation wavelengths cannot be elucidated from these experiments. For each excitation wavelength, a range of conformers are excited, both due to the spectral width of the excitation pulse and due to the overlap of the absorption spectra of the continuum of conformers. Based on chemical intuition and with support from the TD-DFT calculations presented in Figure 5.4, it can be assumed that the lowest energy absorption band of the pentacene dimers corresponds to a more conjugated conformer where the pentacene units are more coplanar. A coplanar geometry is likely to have stronger electronic coupling between the pentacene units, which is in accordance with the observation of faster SF and triplet decay when exciting in the lowest energy absorption band. The species

showing slower SF and triplet depopulation can, with the same arguments, be assigned to a more twisted conformer with weaker electronic coupling between the pentacene units.

5.2 Effect of Excited State Relaxation

The results presented in Figure 5.5 show how the static conformation of a pentacene dimer controls the rate of SF and triplet depopulation in a frozen solution of 2-methyltetrahydrofuran (MTHF) close to the glass transition temperature. In this virtually solid environment, each molecule is locked in a certain conformation and the chromophores cannot rotate or reorient. However, in a liquid environment, the molecule can undergo conformational changes driven by Brownian motion, both in the ground state and in the excited states. In the excited state, conformational reorientation can also result from energy relaxation when the molecule adapts its geometry to a new potential energy surface, as illustrated in Figure 2.4. In order to evaluate how *intra*molecular SF and triplet depopulation is affected by or dependent on dynamic rotation and relaxation in the excited state, the SF kinetics of the pentacene dimers dissolved in liquid solution was compared to when dissolved in a solid polymer film. Figure 5.6 shows single wavelength time traces of the fsTA signal at 505 nm for **PD3** in a liquid toluene solution and in a solid polystyrene film. As described above, this wavelength in the TA spectrum corresponds to the ESA of the T_1T_1 state. The formation of the triplet pair by *intra*molecular SF is similar for both samples with time constants of 28 ps and 46 ps for the toluene solution and polystyrene film, respectively. In contrast, the decay of the triplet state is approximately 40 times slower in the solid film compared to the liquid solution. Similar results were observed also for **PD1** and **PD2**, as shown in Paper IV. The excitation wavelength of 612 nm used in this experiment likely excites a broad range of conformers, because the vibrational progression of each conformer´s electronic transition overlap at shorter wavelengths. Hence, the SF kinetics observed here is an average of all present conformers. The result indicates that the process of triplet pair formation by *intra*molecular SF does not require any conformational changes in the S_1S_0 excited state and can occur in the molecular geometry of the ground state. In contrast, the slower rate of

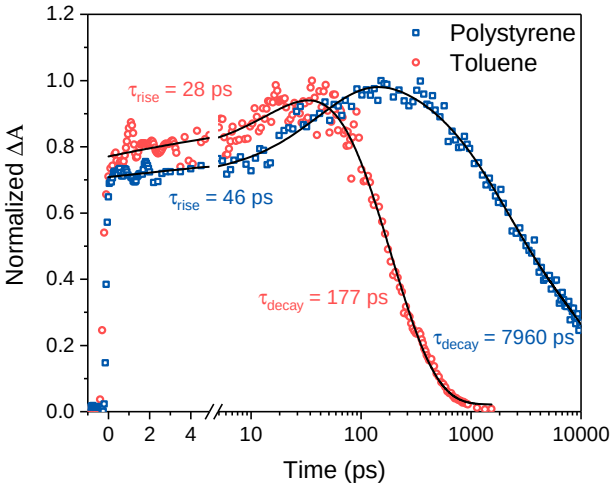

Figure 5.6: Time evolution of the fsTA signal at the 505 nm ESA band, corresponding to the T_1T_1 state, for **PD3**. Measured at room temperature in toluene solution and in solid polystyrene film, excitation wavelength 612 nm. Black lines show fit to a sum of exponentials, $\Delta A = \sum_i a_i e^{-t/\tau_i}$ and the obtained time constants, τ, are shown in the graph.

triplet decay in the solid sample indicates that decay by triplet recombination is only efficient in some geometries with strong coupling between the pentacene units. Therefore, the triplet pair formed in conformers with weaker electronic coupling requires conformational reorientation in the excited state to find a geometry where it can decay by fast triplet recombination.

5.3 Summary of Intramolecular Singlet Fission

The results presented in this chapter have shown how the orientation of chromophores controls the rate of *intra*molecular SF and how conformational reorientation in the excited state governs fast decay of the triplet pair. The conformational effects have a major influence, in fact, the rate of SF and triplet pair decay can vary with more than three orders of magnitude depending on the geometry of the molecule. Hence, the exact geometry of the SF chromophores is a design parameter that cannot be neglected in the development of new molecular systems for SF. Further, the results presented in Figure 5.6 show that conformational flexibility in the excited state has a large influence on the rate of triplet decay, but not on the SF process in this case. This indicates that the SF and triplet recombination processes have different dependencies on the electronic coupling between the chromophores. As described in Section 2.3, the electronic coupling between the chromophores is often seen as a parameter that must be fine-tuned to balance between efficient SF and long-lived triplets. The insight that the SF process is less susceptible to molecular reorientation than triplet recombination is important because it opens up for designing new molecular systems that show both efficient SF and long-lived triplets. In conclusion, both the static chromophore orientation as well as dynamic conformation flexibility must be considered and optimized in the development of new efficient systems for *intra*molecular SF.

6

Concluding Remarks and Outlook

The work presented in this thesis has focused on investigating the mechanisms behind PUC and SF with a long-term goal of making PUC and SF applicable in solar energy technologies. Design of *intra*molecular PUC and SF systems have been used as an approach for enabling efficient PUC and SF in solid-state materials. This thesis have described the challenges associated with the transformation of the photophysical processes governing PUC and SF, from electronic interactions enabled by diffusion of individual molecules in solution to *intra*molecular interactions within a molecular construct.

The results presented in this thesis has shown that the electronic interactions governing PUC and SF can be very sensitive to the relative orientation of the chromophores. This is because the molecular geometry determines the strength and nature of the electronic coupling between the chromophores. By studying the electronic interaction in well-defined *intra*molecular systems, detailed information about the photophysical processes have been achieved that could not have been obtained by studying the corresponding *inter*molecular interactions of individual molecules in solutions. It has in this thesis been demonstrated that the rate of *intra*molecular excitation energy transfer within a sensitizer-annihilator complex depends heavily on the coordination geometry. Further, it has been shown that the relative orientation of the SF chromophores in a dimer determines the rate of both triplet pair formation by SF and the rate of triplet pair decay. This insight provides new design criteria for the development of novel efficient PUC and SF systems.

For both PUC and SF, *intra*molecular interactions have the benefit that it enables fast energy transfer processes beyond the limitation of molecular diffusion. However, it comes with the drawback that it invokes additional quenching processes that are typically not observed in the corresponding *inter*molecular system in solution. For PUC, coordination of the sensitizer to the annihilator enables excitation energy back transfer, both on the triplet and singlet surface, which quenches the overall PUC process. For SF, the close proximity of the chromophores hinders decorrelation of the triplet pair into free triplets, which results in short excited state lifetime and limited usability of the generated triplet excitons. However, a careful design of the molecular constructs could potentially reduce the influence of these quenching processes. For example, a large chromophore network would enable excitons in the network to interact and dissociate by exciton migration. This would hence mimic the *inter*molecular system in solution, but where the diffusion of excited molecules has been replaced by *intra*molecular exciton migration. The annihilator dendrimers and large particles of annihilator polymers presented in Chapter 4 is a step on the way to such an *intra*molecular PUC system.

The concepts of PUC and SF are mechanistically closely related, but has to a large extent developed as separate research fields. Comparing the research fields of PUC and SF, PUC is a more mature technique and it is not unlikely that it will reach a breakthrough of implementation of PUC into viable products within some few years. There are still many things that are unknown and many challenges to address. For example, the details of the spin statistics in TTA, which set an upper limit on the upconversion emission quantum yield, is not fully understood for *inter*molecular TTA and even less studied for *intra*molecular TTA. A challenge for large scale implementation of PUC in solar energy devices is the development of novel sensitizers and annihilators that are stable over time and, preferably, only containing earth abundant elements. The chromophores must also absorb and emit photons in a wavelength range that is suitable for the application of interest. SF as a research field is further away from real world applications, even though it has developed a lot during the past years and we have now a much better mechanistic insight in the SF process than only some years ago. With the massive growth of the PUC and SF research fields the past years and the high pace of scientific achievements, there are good chances of successful implementation of photon energy conversion technologies into future solar energy devices.

7
Acknowledgements

First of all I would like to thank my supervisor Bo Albinsson. Thank you for giving me the opportunity to work as a PhD student in your group. Thank you for believing in me. Also thanks to my co-supervisor Maria Abrahamsson and examiner Jerker Mårtensson.

I would also like to thank all the collaborators whose work have enabled our research projects.

Thanks to all former and present members of our spectroscopy group for the interesting discussions and good fika. Thanks to Maria, Joakim, Gaowa, Deise, Lili, Andrew and Liam. I have learned a lot from you.

A special thanks to:

Victor for introducing me to the world of upconversion and for helping me during my first year as a PhD student.

Betül for introducing me to the world of lasers. Your endless support and positive attitude have shown me more sides of what it means to be a good scientist. It is always fun to work with you in the lab and I am happy to have you as a friend.

Elin for all the help and guidance throughout the time as a PhD student. Thanks for all the funny moments during the conferences.

Axel for all the interesting and spontaneous discussions.

Rasmus for your endless smile. Thanks for all the fun times in the lab. Thanks for your patience, both with the lasers in the lab and with me when I am disturbing you in your office.

Wera and Jesper for being the most wonderful office mates I could imagine. It is the open, friendly, supporting and positive atmosphere you create in our office that makes it fun to go to work.

All other people on floor five for the great atmosphere and positive work environment you create.

Thanks again to Andrew, Liam, Wera and Rasmus for proofreading this thesis.

Bibliography

[1] ICCP, 2021. Climate change 2021: The physical science basis. contribution of working group i to the sixth assessment report of the intergovernmental panel on climate change. Masson-Delmotte, V., P. Zhai, A. Pirani, S.L. Connors, C. Péan, S. Berger, N. Caud, Y. Chen, L. Goldfarb, M.I. Gomis, M. Huang, K. Leitzell, E. Lonnoy, J.B.R. Matthews, T.K. Maycock, T. Waterfield, O. Yelekçi, R. Yu, and B. Zhou (eds.). Cambridge University Press. In Press.

[2] T. M. Letcher. 1 - Why Solar Energy? In T. M. Letcher and V. M. Fthenakis, editors, *A Comprehensive Guide to Solar Energy Systems*, chapter 1, pages 3–16. Academic Press, 2018.

[3] International Energy Agency. Key world energy statistics 2020. https://iea.blob.core.windows.net/assets/1b7781df-5c93-492a-acd6-01fc90388b0f/Key_World_Energy_Statistics_2020.pdf. Accessed 2021-10-08.

[4] W. Shockley and H. J. Queisser. Detailed Balance Limit of Efficiency of p-n Junction Solar Cells. *Journal of Applied Physics*, 32(3):510–519, 1961.

[5] M. D. Archer and J. R. Bolton. Requirements for ideal performance of photochemical and photovoltaic solar energy converters. *Journal of Physical Chemistry*, 94(21):8028–8036, 1990.

[6] M. C. Hanna and A. J. Nozik. Solar conversion efficiency of photovoltaic and photoelectrolysis cells with carrier multiplication absorbers. *Journal of Applied Physics*, 100(7):74510, 2006.

[7] National Renewable Energy Laboratory. Reference air mass 1.5 spectra. `https://www.nrel.gov/grid/solar-resource/spectra-am1.5.html`. Accessed: 2021-10-25.

[8] C. A. Parker and C. G. Hatchard. Delayed fluorescence from solutions of anthracene and phenanthrene. *Proceedings of the Royal Society of London. Series A. Mathematical and Physical Sciences*, 269(1339):574–584, 1962.

[9] P. Gibart, F. Auzel, J.-C. Guillaume, and K. Zahraman. Below Band-Gap IR Response of Substrate-Free GaAs Solar Cells Using Two-Photon Up-Conversion. *Japanese Journal of Applied Physics*, 35(8):4401–4402, 1996.

[10] T. Trupke, M. A. Green, and P. Würfel. Improving solar cell efficiencies by up-conversion of sub-band-gap light. *Journal of Applied Physics*, 92(7):4117–4122, 2002.

[11] R. R. Islangulov, J. Lott, C. Weder, and F. N. Castellano. Noncoherent Low-Power Upconversion in Solid Polymer Films. *Journal of the American Chemical Society*, 129(42):12652–12653, 2007.

[12] T. Trupke, A. Shalav, B. S. Richards, P. Würfel, and M. A. Green. Efficiency enhancement of solar cells by luminescent up-conversion of sunlight. *Solar Energy Materials and Solar Cells*, 90(18):3327–3338, 2006.

[13] S. Rühle. Tabulated values of the Shockley–Queisser limit for single junction solar cells. *Solar Energy*, 130:139–147, 2016.

[14] K. Börjesson, D. Dzebo, B. Albinsson, and K. Moth-Poulsen. Photon upconversion facilitated molecular solar energy storage. *Journal of Materials Chemistry A*, 1(30):8521–8524, 2013.

[15] C. Simpson, T. M. Clarke, R. W. MacQueen, Y. Y. Cheng, A. J. Trevitt, A. J. Mozer, P. Wagner, T. W. Schmidt, and A. Nattestad. An intermediate band dye-sensitised solar cell using triplet–triplet annihilation. *Physical Chemistry Chemical Physics*, 17(38):24826–24830, 2015.

[16] Y. Y. Cheng, A. Nattestad, T. F. Schulze, R. W. MacQueen, B. Fuckel, K. Lips, G. G. Wallace, T. Khoury, M. J. Crossley, and T. W. Schmidt. Increased upconversion performance for thin film solar cells: a trimolecular composition. *Chemical Science*, 7(1):559–568, 2016.

[17] Y. L. Lin, M. Koch, A. N. Brigeman, D. M. E. Freeman, L. Zhao, H. Bronstein, N. C. Giebink, G. D. Scholes, and B. P. Rand. Enhanced sub-bandgap efficiency of a solid-state organic intermediate band solar cell using triplet–triplet annihilation. *Energy & Environmental Science*, 10(6):1465–1475, 2017.

[18] D. Beery, J. P. Wheeler, A. Arcidiacono, and K. Hanson. CdSe Quantum Dot Sensitized Molecular Photon Upconversion Solar Cells. *ACS Applied Energy Materials*, 3(1):29–37, 2020.

[19] D. Beery, T. W. Schmidt, and K. Hanson. Harnessing Sunlight via Molecular Photon Upconversion. *ACS Applied Materials & Interfaces*, 13(28):32601–32605, 2021.

[20] S. Hoseinkhani, R. Tubino, F. Meinardi, and A. Monguzzi. Achieving the photon upconversion thermodynamic yield upper limit by sensitized triplet-triplet annihilation. *Physical Chemistry Chemical Physics*, 17(6):4020–4024, 2015.

[21] W. Sun, A. Ronchi, T. Zhao, J. Han, A. Monguzzi, and P. Duan. Highly efficient photon upconversion based on triplet–triplet annihilation from bichromophoric annihilators. *Journal of Materials Chemistry C*, 9:14201–14208, 2021.

[22] L. Frazer, J. K. Gallaher, and T. W. Schmidt. Optimizing the Efficiency of Solar Photon Upconversion. *ACS Energy Letters*, 2(6):1346–1354, 2017.

[23] V. Gray, K. Moth-Poulsen, B. Albinsson, and M. Abrahamsson. Towards efficient solid-state triplet–triplet annihilation based photon upconversion: Supramolecular, macromolecular and self-assembled systems. *Coordination Chemistry Reviews*, 362:54–71, 2018.

[24] J.-H. Kim, F. Deng, F. N. Castellano, and J.-H. Kim. High Efficiency Low-Power Upconverting Soft Materials. *Chemistry of Materials*, 24(12):2250–2252, 2012.

[25] D. F. Barbosa de Mattos, A. Dreos, M. D. Johnstone, A. Runemark, C. Sauvée, V. Gray, K. Moth-Poulsen, H. Sundén, and M. Abrahamsson. Covalent incorporation of diphenylanthracene in oxotriphenylhexanoate organogels as a quasi-solid photon upconversion matrix. *The Journal of Chemical Physics*, 153(21):214705, 2020.

[26] P. Bharmoria, S. Hisamitsu, Y. Sasaki, T. S. Kang, M.-a. Morikawa, B. Joarder, K. Moth-Poulsen, H. Bildirir, A. Mårtensson, N. Yanai, and N. Kimizuka. Photon upconverting bioplastics with high efficiency and in-air durability. *Journal of Materials Chemistry C*, 9:11655–11661, 2021.

[27] A. Monguzzi, M. Mauri, A. Bianchi, M. K. Dibbanti, R. Simonutti, and F. Meinardi. Solid-State Sensitized Upconversion in Polyacrylate Elastomers. *The Journal of Physical Chemistry C*, 120(5):2609–2614, 2016.

[28] T. Mizokuro, A. Abulikemu, K. Suzuki, Y. Sakagami, R. Nishii, T. Jin, and K. Kamada. Triplet–triplet annihilation upconversion through triplet energy transfer at a nanoporous solid–liquid interface. *Physical Chemistry Chemical Physics*, 22(32):17807–17813, 2020.

[29] F. Saenz, A. Ronchi, M. Mauri, R. Vadrucci, F. Meinardi, A. Monguzzi, and C. Weder. Nanostructured Polymers Enable Stable and Efficient Low-Power Photon Upconversion. *Advanced Functional Materials*, 31(1):2004495, 2021.

[30] K. R. Parenti, G. He, S. N. Sanders, A. B. Pun, E. Kumarasamy, M. Y. Sfeir, and L. M. Campos. Bridge Resonance Effects in Singlet Fission. *The Journal of Physical Chemistry A*, 124(45):9392–9399, 2020.

[31] B. Ehrler, K. P. Musselman, M. L. Böhm, R. H. Friend, and N. C. Greenham. Hybrid pentacene/a-silicon solar cells utilizing multiple carrier generation via singlet exciton fission. *Applied Physics Letters*, 101(15):153507, 2012.

[32] D. N. Congreve, J. Lee, N. J. Thompson, E. Hontz, S. R. Yost, P. D. Reusswig, M. E. Bahlke, S. Reineke, T. Van Voorhis, and M. A. Baldo. External quantum efficiency above 100singlet-exciton-fission–based organic photovoltaic cell. *Science*, 340(6130):334–337, 2013.

[33] T. Banerjee, S. P. Hill, M. A. Hermosilla-Palacios, B. D. Piercy, J. Haney, B. Casale, A. E. DePrince, M. D. Losego, V. D. Kleiman, and K. Hanson. Diphenylisobenzofuran Bound to Nanocrystalline Metal Oxides: Excimer Formation, Singlet Fission, Electron Injection, and Low Energy Sensitization. *The Journal of Physical Chemistry C*, 122(50):28478–28490, 2018.

[34] M. Einzinger, T. Wu, J. F. Kompalla, H. L. Smith, C. F. Perkinson, L. Nienhaus, S. Wieghold, D. N. Congreve, A. Kahn, M. G. Bawendi, and M. A. Baldo. Sensitization of silicon by singlet exciton fission in tetracene. *Nature*, 571(7763):90–94, 2019.

[35] E. Sundin, R. Ringström, F. Johansson, B. Küçüköz, A. Ekebergh, V. Gray, B. Albinsson, J. Mårtensson, and M. Abrahamsson. Singlet Fission and Electron Injection from the Triplet Excited State in Diphenylisobenzofuran–Semiconductor Assemblies: Effects of Solvent Polarity and Driving Force. *The Journal of Physical Chemistry C*, 124(38):20794–20805, 2020.

[36] N. J. Thompson, M. W. B. Wilson, D. N. Congreve, P. R. Brown, J. M. Scherer, T. S. Bischof, M. Wu, N. Geva, M. Welborn, T. V. Voorhis, V. Bulović, M. G. Bawendi, and M. A. Baldo. Energy harvesting of non-emissive triplet excitons in tetracene by emissive PbS nanocrystals. *Nature Materials*, 13(11):1039–1043, 2014.

[37] J. R. Allardice, A. Thampi, S. Dowland, J. Xiao, V. Gray, Z. Zhang, P. Budden, A. J. Petty, N. J. L. K. Davis, N. C. Greenham, J. E. Anthony, and A. Rao. Engineering Molecular Ligand Shells on Quantum Dots for Quantitative Harvesting of Triplet Excitons Generated by Singlet Fission. *Journal of the American Chemical Society*, 141(32):12907–12915, 2019.

[38] V. Gray, J. R. Allardice, Z. Zhang, S. Dowland, J. Xiao, A. J. Petty, J. E. Anthony, N. C. Greenham, and A. Rao. Direct vs Delayed Triplet Energy Transfer from Organic Semiconductors to Quantum Dots and Implications for Luminescent Harvesting of Triplet Excitons. *ACS Nano*, 14(4):4224–4234, 2020.

[39] S. Singh, W. J. Jones, W. Siebrand, B. P. Stoicheff, and W. G. Schneider. Laser Generation of Excitons and Fluorescence in Anthracene Crystals. *The Journal of Chemical Physics*, 42(1):330–342, 1965.

[40] C. E. Swenberg and W. T. Stacy. Bimolecular radiationless transitions in crystalline tetracene. *Chemical Physics Letters*, 2(5):327–328, 1968.

[41] N. Geacintov, M. Pope, and F. Vogel. Effect of Magnetic Field on the Fluorescence of Tetracene Crystals: Exciton Fission. *Physical Review Letters*, 22(12):593–596, 1969.

[42] B. J. Walker, A. J. Musser, D. Beljonne, and R. H. Friend. Singlet exciton fission in solution. *Nature Chemistry*, 5:1019, 2013.

[43] A. M. Müller, Y. S. Avlasevich, W. W. Schoeller, K. Müllen, and C. J. Bardeen. Exciton Fission and Fusion in Bis(tetracene) Molecules with Different Covalent Linker Structures. *Journal of the American Chemical Society*, 129(46):14240–14250, 2007.

[44] J. Zirzlmeier, D. Lehnherr, P. B. Coto, E. T. Chernick, R. Casillas, B. S. Basel, M. Thoss, R. R. Tykwinski, and D. M. Guldi. Singlet fission in pentacene dimers. *Proceedings of the National Academy of Sciences*, 112(17):5325–5330, 2015.

[45] I. Papadopoulos, J. Zirzlmeier, C. Hetzer, Y. J. Bae, M. D. Krzyaniak, M. R. Wasielewski, T. Clark, R. R. Tykwinski, and D. M. Guldi. Varying the Interpentacene Electronic Coupling to Tune Singlet Fission. *Journal of the American Chemical Society*, 141(15):6191–6203, 2019.

[46] T. Yamakado, S. Takahashi, K. Watanabe, Y. Matsumoto, A. Osuka, and S. Saito. Conformational Planarization versus Singlet Fission: Distinct Excited-State Dynamics of Cyclooctatetraene-Fused Acene Dimers. *Angewandte Chemie International Edition*, 57(19):5438–5443, 2018.

[47] K. Shizu, C. Adachi, and H. Kaji. Effect of Vibronic Coupling on Correlated Triplet Pair Formation in the Singlet Fission Process of Linked Tetracene Dimers. *The Journal of Physical Chemistry A*, 124(18):3641–3651, 2020.

[48] A. Aster, F. Zinna, C. Rumble, J. Lacour, and E. Vauthey. Singlet Fission in a Flexible Bichromophore with Structural and Dynamic Control. *Journal of the American Chemical Society*, 143(5):2361–2371, 2021.

[49] C. Hetzer, D. M. Guldi, and R. R. Tykwinski. Pentacene Dimers as a Critical Tool for the Investigation of Intramolecular Singlet Fission. *Chemistry – A European Journal*, 24(33):8245–8257, 2018.

[50] T. C. Berkelbach, M. S. Hybertsen, and D. R. Reichman. Microscopic theory of singlet exciton fission. II. Application to pentacene dimers and the role of superexchange. *The Journal of Chemical Physics*, 138(11):114103, 2013.

[51] L. M. Yablon, S. N. Sanders, K. Miyazaki, E. Kumarasamy, G. He, B. Choi, N. Ananth, M. Sfeir, and L. Campos. Singlet Fission and Triplet Pair Recombination in Bipentacenes with a Twist. *Materials Horizons*, 2021. http://dx.doi.org/10.1039/D1MH01201K.

[52] H. Sakai, R. Inaya, H. Nagashima, S. Nakamura, Y. Kobori, N. V. Tkachenko, and T. Hasobe. Multiexciton Dynamics Depending on Intramolecular Orientations in Pentacene Dimers: Recombination and Dissociation of Correlated Triplet Pairs. *The Journal of Physical Chemistry Letters*, 9(12):3354–3360, 2018.

[53] S. Nakamura, H. Sakai, H. Nagashima, M. Fuki, K. Onishi, R. Khan, Y. Kobori, N. V. Tkachenko, and T. Hasobe. Synergetic Role of Conformational Flexibility and Electronic Coupling for Quantitative Intramolecular Singlet Fission. *The Journal of Physical Chemistry C*, 125(33):18287–18296, 2021.

[54] P. Atkins and R. Friedman. *Molecular Quantum Mechanics*. OUP Oxford, 2011.

[55] G. N. Lewis and M. Kasha. Phosphorescence and the triplet state. *Journal of the American Chemical Society*, 66(12):2100–2116, 1944.

[56] T. Forster. Energiewanderung und fluoreszenz. *Naturwissenschaften*, 33(6):166–175, 1946.

[57] N. J. Turro. *Modern molecular photochemistry*. University science books, Sausalito, California, USA, 1991.

[58] Y. Zhou, F. N. Castellano, T. W. Schmidt, and K. Hanson. On the Quantum Yield of Photon Upconversion via Triplet–Triplet Annihilation. *ACS Energy Letters*, 5(7):2322–2326, 2020.

[59] IUPAC. Compendium of chemical terminology, 2nd ed. (the "gold book"). Blackwell Scientific Publications, Oxford (1997). Online version (2019-) created by S. J. Chalk. ISBN 0-9678550-9-8. https://doi.org/10.1351/goldbook.

[60] R. E. Merrifield. Theory of magnetic field effects on the mutual annihilation of triplet excitons. *The Journal of Chemical Physics*, 48(9):4318–4319, 1968.

[61] T. N. Singh-Rachford and F. N. Castellano. Photon upconversion based on sensitized triplet–triplet annihilation. *Coordination Chemistry Reviews*, 254(21):2560–2573, 2010.

[62] Y. Y. Cheng, B. Fückel, T. Khoury, R. G. C. R. Clady, M. J. Y. Tayebjee, N. J. Ekins-Daukes, M. J. Crossley, and T. W. Schmidt. Kinetic Analysis of Photochemical Upconversion by Triplet-Triplet Annihilation: Beyond Any Spin Statistical Limit. *The Journal of Physical Chemistry Letters*, 1(12):1795–1799, 2010.

[63] D. G. Bossanyi, M. Matthiesen, S. Wang, J. A. Smith, R. C. Kilbride, J. D. Shipp, D. Chekulaev, E. Holland, J. E. Anthony, J. Zaumseil, A. J. Musser, and J. Clark. Emissive spin-0 triplet-pairs are a direct product of triplet–triplet annihilation in pentacene single crystals and anthradithiophene films. *Nature Chemistry*, 13(2):163–171, 2021.

[64] A. Monguzzi, J. Mezyk, F. Scotognella, R. Tubino, and F. Meinardi. Upconversion-induced fluorescence in multicomponent systems: Steady-state excitation power threshold. *Physical Review B*, 78(19):195112, 2008.

[65] Y. Y. Cheng, T. Khoury, R. G. C. R. Clady, M. J. Y. Tayebjee, N. J. Ekins-Daukes, M. J. Crossley, and T. W. Schmidt. On the efficiency limit of triplet-triplet annihilation for photochemical upconversion. *Physical Chemistry Chemical Physics*, 12(1):66–71, 2010.

[66] A. Haefele, J. Blumhoff, R. S. Khnayzer, and F. N. Castellano. Getting to the (Square) Root of the Problem: How to Make Noncoherent Pumped Upconversion Linear. *The Journal of Physical Chemistry Letters*, 3(3):299–303, 2012.

[67] J. N. Schrauben, Y. Zhao, C. Mercado, P. I. Dron, J. L. Ryerson, J. Michl, K. Zhu, and J. C. Johnson. Photocurrent Enhanced by Singlet Fission in a Dye-Sensitized Solar Cell. *ACS Applied Materials & Interfaces*, 7(4):2286–2293, 2015.

[68] S. W. Eaton, L. E. Shoer, S. D. Karlen, S. M. Dyar, E. A. Margulies, B. S. Veldkamp, C. Ramanan, D. A. Hartzler, S. Savikhin, T. J. Marks, and M. R. Wasielewski. Singlet Exciton Fission in Polycrystalline Thin Films of a Slip-Stacked Perylenediimide. *Journal of the American Chemical Society*, 135(39):14701–14712, 2013.

[69] M. Chen, N. E. Powers-Riggs, A. F. Coleman, R. M. Young, and M. R. Wasielewski. Singlet Fission in Quaterrylenediimide Thin Films. *The Journal of Physical Chemistry C*, 124(5):2791–2798, 2020.

[70] A. K. Le, J. A. Bender, and S. T. Roberts. Slow Singlet Fission Observed in a Polycrystalline Perylenediimide Thin Film. *The Journal of Physical Chemistry Letters*, 7(23):4922–4928, 2016.

[71] N. V. Korovina, J. Joy, X. Feng, C. Feltenberger, A. I. Krylov, S. E. Bradforth, and M. E. Thompson. Linker-Dependent Singlet Fission in Tetracene Dimers. *Journal of the American Chemical Society*, 140(32):10179–10190, 2018.

[72] H. Liu, Z. Wang, X. Wang, L. Shen, C. Zhang, M. Xiao, and X. Li. Singlet exciton fission in a linear tetracene tetramer. *Journal of Materials Chemistry C*, 6(13):3245–3253, 2018.

[73] A. Rao, M. W. B. Wilson, J. M. Hodgkiss, S. Albert-Seifried, H. Bässler, and R. H. Friend. Exciton Fission and Charge Generation via Triplet Excitons in Pentacene/C60 Bilayers. *Journal of the American Chemical Society*, 132(36):12698–12703, 2010.

[74] H. Marciniak, I. Pugliesi, B. Nickel, and S. Lochbrunner. Ultrafast singlet and triplet dynamics in microcrystalline pentacene films. *Physical Review B*, 79(23):235318, 2009.

[75] C. Jundt, G. Klein, B. Sipp, J. Le Moigne, M. Joucla, and A. A. Villaeys. Exciton dynamics in pentacene thin films studied by pump-probe spectroscopy. *Chemical Physics Letters*, 241(1):84–88, 1995.

[76] M. Dvořák, S. K. K. Prasad, C. B. Dover, C. R. Forest, A. Kaleem, R. W. MacQueen, A. J. Petty, R. Forecast, J. E. Beves, J. E. Anthony, M. J. Y. Tayebjee, A. Widmer-Cooper, P. Thordarson, and T. W. Schmidt. Singlet Fission in Concentrated TIPS-Pentacene Solutions: The Role of Excimers and Aggregates. *Journal of the American Chemical Society*, 143(34):13749–13758, 2021.

[77] K. Miyata, F. S. Conrad-Burton, F. L. Geyer, and X.-Y. Zhu. Triplet Pair States in Singlet Fission. *Chemical Reviews*, 119(6):4261–4292, 2019.

[78] S. Lukman, K. Chen, J. M. Hodgkiss, D. H. P. Turban, N. D. M. Hine, S. Dong, J. Wu, N. C. Greenham, and A. J. Musser. Tuning the role of charge-transfer states in intramolecular singlet exciton fission through side-group engineering. *Nature Communications*, 7(1):13622, 2016.

[79] B. S. Basel, J. Zirzlmeier, C. Hetzer, S. R. Reddy, B. T. Phelan, M. D. Krzyaniak, M. K. Volland, P. B. Coto, R. M. Young, T. Clark, M. Thoss, R. R. Tykwinski, M. R. Wasielewski, and D. M. Guldi. Evidence for Charge-Transfer Mediation in the Primary Events of Singlet Fission in a Weakly Coupled Pentacene Dimer. *Chem*, 4(5):1092–1111, 2018.

[80] A. M. Alvertis, S. Lukman, T. J. H. Hele, E. G. Fuemmeler, J. Feng, J. Wu, N. C. Greenham, A. W. Chin, and A. J. Musser. Switching between Coherent and Incoherent Singlet Fission via Solvent-Induced Symmetry Breaking. *Journal of the American Chemical Society*, 141(44):17558–17570, 2019.

[81] E. G. Fuemmeler, S. N. Sanders, A. B. Pun, E. Kumarasamy, T. Zeng, K. Miyata, M. L. Steigerwald, X.-Y. Zhu, M. Y. Sfeir, L. M. Campos, and N. Ananth. A Direct Mechanism of Ultrafast Intramolecular Singlet Fission in Pentacene Dimers. *ACS Central Science*, 2(5):316–324, 2016.

[82] J. Zirzlmeier, R. Casillas, S. R. Reddy, P. B. Coto, D. Lehnherr, E. T. Chernick, I. Papadopoulos, M. Thoss, R. R. Tykwinski, and D. M. Guldi. Solution-based intramolecular singlet fission in cross-conjugated pentacene dimers. *Nanoscale*, 8(19):10113–10123, 2016.

[83] H. L. Stern, A. J. Musser, S. Gelinas, P. Parkinson, L. M. Herz, M. J. Bruzek, J. Anthony, R. H. Friend, and B. J. Walker. Identification of a triplet pair intermediate in singlet ex-

citon fission in solution. *Proceedings of the National Academy of Sciences*, 112(25):7656–7661, 2015.

[84] A. B. Pun, A. Asadpoordarvish, E. Kumarasamy, M. J. Y. Tayebjee, D. Niesner, D. R. McCamey, S. N. Sanders, L. M. Campos, and M. Y. Sfeir. Ultra-fast intramolecular singlet fission to persistent multiexcitons by molecular design. *Nature Chemistry*, 11(9):821–828, 2019.

[85] L. R. Weiss, S. L. Bayliss, F. Kraffert, K. J. Thorley, J. E. Anthony, R. Bittl, R. H. Friend, A. Rao, N. C. Greenham, and J. Behrends. Strongly exchange-coupled triplet pairs in an organic semiconductor. *Nature Physics*, 13(2):176–181, 2017.

[86] M. J. Y. Tayebjee, S. N. Sanders, E. Kumarasamy, L. M. Campos, M. Y. Sfeir, and D. R. McCamey. Quintet multiexciton dynamics in singlet fission. *Nature Physics*, 13(2):182–188, 2017.

[87] G. D. Scholes. Correlated Pair States Formed by Singlet Fission and Exciton–Exciton Annihilation. *The Journal of Physical Chemistry A*, 119(51):12699–12705, 2015.

[88] M. B. Smith and J. Michl. Singlet fission. *Chemical Reviews*, 110(11):6891–6936, 2010.

[89] Z. Havlas and J. Michl. Guidance for Mutual Disposition of Chromophores for Singlet Fission. *Israel Journal of Chemistry*, 56(1):96–106, 2016.

[90] E. A. Buchanan and J. Michl. Packing Guidelines for Optimizing Singlet Fission Matrix Elements in Noncovalent Dimers. *Journal of the American Chemical Society*, 139(44):15572–15575, 2017.

[91] P. E. Hartnett, E. A. Margulies, C. M. Mauck, S. A. Miller, Y. Wu, Y.-L. Wu, T. J. Marks, and M. R. Wasielewski. Effects of Crystal Morphology on Singlet Exciton Fission in Diketopyrrolopyrrole Thin Films. *The Journal of Physical Chemistry B*, 120(7):1357–1366, 2016.

[92] S. Khan and S. Mazumdar. Free Triplets Versus Bound Triplet–Triplet Biexciton in Intramolecular Singlet Fission Materials: Structure–Property Correlations. *The Journal of Physical Chemistry C*, 124(1):1171–1177, 2020.

[93] R. D. Pensack, A. J. Tilley, C. Grieco, G. E. Purdum, E. E. Ostroumov, D. B. Granger, D. G. Oblinsky, J. C. Dean, G. S. Doucette, J. B. Asbury, Y.-L. Loo, D. S. Seferos, J. E. Anthony, and G. D. Scholes. Striking the right balance of intermolecular coupling for high-efficiency singlet fission. *Chemical Science*, 9(29):6240–6259, 2018.

[94] D. R. James, D. R. M. Demmer, R. E. Verrall, and R. P. Steer. Excitation pulse-shape mimic technique for improving picosecond-laser-excited time-correlated single-photon counting deconvolutions. *Review of Scientific Instruments*, 54(9):1121–1130, 1983.

[95] S. M. Bachilo and R. B. Weisman. Determination of Triplet Quantum Yields from Triplet-Triplet Annihilation Fluorescence. *The Journal of Physical Chemistry A*, 104(33):7711–7714, 2000.

[96] D. C. Lay. *Linear algebra and its application*. Pearson Education, Boston, MA, USA, third edition, 2006.

[97] M. Kubista, R. Sjoeback, and B. Albinsson. Determination of equilibrium constants by chemometric analysis of spectroscopic data. *Analytical Chemistry*, 65(8):994–998, 1993.

[98] I. H. M. van Stokkum, D. S. Larsen, and R. van Grondelle. Global and target analysis of time-resolved spectra. *Biochimica et Biophysica Acta (BBA) - Bioenergetics*, 1657(2):82–104, 2004.

[99] C. Ruckebusch, M. Sliwa, P. Pernot, A. de Juan, and R. Tauler. Comprehensive data analysis of femtosecond transient absorption spectra: A review. *Journal of Photochemistry and Photobiology C: Photochemistry Reviews*, 13(1):1–27, 2012.

[100] A. Szabo and N. Ostlund. *Modern Quantum Chemistry: Introduction to Advanced Electronic Structure Theory*. Dover Books on Chemistry. Dover Publications, 2012.

[101] M. J. Frisch, G. W. Trucks, H. B. Schlegel, G. E. Scuseria, M. A. Robb, J. R. Cheeseman, G. Scalmani, V. Barone, G. A. Petersson, H. Nakatsuji, X. Li, M. Caricato, A. V. Marenich, J. Bloino, B. G. Janesko, R. Gomperts, B. Mennucci, H. P. Hratchian, J. V. Ortiz, A. F. Izmaylov, J. L. Sonnenberg, D. Williams-Young, F. Ding, F. Lipparini, F. Egidi, J. Goings, B. Peng, A. Petrone, T. Henderson, D. Ranasinghe, V. G. Zakrzewski, J. Gao, N. Rega, G. Zheng, W. Liang, M. Hada, M. Ehara, K. Toyota, R. Fukuda, J. Hasegawa, M. Ishida, T. Nakajima, Y. Honda, O. Kitao, H. Nakai, T. Vreven, K. Throssell, J. A. Montgomery, Jr., J. E. Peralta, F. Ogliaro, M. J. Bearpark, J. J. Heyd, E. N. Brothers, K. N. Kudin, V. N. Staroverov, T. A. Keith, R. Kobayashi, J. Normand, K. Raghavachari, A. P. Rendell, J. C. Burant, S. S. Iyengar, J. Tomasi, M. Cossi, J. M. Millam, M. Klene, C. Adamo, R. Cammi, J. W. Ochterski, R. L. Martin, K. Morokuma, O. Farkas, J. B. Foresman, and D. J. Fox. Gaussian∼16 Revision A.03, 2016. Gaussian Inc. Wallingford CT.

[102] P. Hohenberg and W. Kohn. Inhomogeneous Electron Gas. *Physical Review*, 136(3B):B864–B871, 1964.

[103] N. D. Woods, M. C. Payne, and P. J. Hasnip. Computing the self-consistent field in Kohn–Sham density functional theory. *Journal of Physics: Condensed Matter*, 31(45):453001, 2019.

[104] V. Gray, B. Küçüköz, F. Edhborg, M. Abrahamsson, K. Moth-Poulsen, and B. Albinsson. Singlet and Triplet Energy Transfer Dynamics in Self-Assembled Axial Porphyrin-Anthracene Complexes: Towards Supra-molecular Structures for Photon Upconversion. *Physical Chemistry Chemical Physics*, 20(11):7549–7558, 2018.

[105] F. Edhborg, B. Küçüköz, V. Gray, and B. Albinsson. Singlet Energy Transfer in Anthracene–Porphyrin Complexes: Mechanism, Geometry, and Implications for Intramolecular Photon Upconversion. *The Journal of Physical Chemistry B*, 123(46):9934–9943, 2019.

[106] F. Edhborg, H. Bildirir, P. Bharmoria, K. Moth-Poulsen, and B. Albinsson. Intramolecular Triplet–Triplet Annihilation Photon Upconversion in Diffusionally Restricted Anthracene Polymer. *The Journal of Physical Chemistry B*, 125(23):6255–6263, 2021.

[107] V. Gray, K. Börjesson, D. Dzebo, M. Abrahamsson, B. Albinsson, and K. Moth-Poulsen. Porphyrin–Anthracene Complexes: Potential in Triplet–Triplet Annihilation Upconversion. *The Journal of Physical Chemistry C*, 120(34):19018–19026, 2016.

[108] J. Andraos. A streamlined approach to solving simple and complex kinetic systems analytically. *Journal of Chemical Education*, 76(11):1578, 1999.

[109] J. Mårtensson. Calculation of the Förster orientation factor for donor-acceptor systems with one chromophore of threefold or higher symmetry: zinc porphyrin. *Chemical Physics Letters*, 229(4):449–456, 1994.

[110] Y. Matsui, M. Kanoh, E. Ohta, T. Ogaki, and H. Ikeda. Triplet–Triplet Annihilation-Photon Upconversion Employing an Adamantane-linked Diphenylanthracene Dyad Strategy. *Journal of Photochemistry and Photobiology A: Chemistry*, 387:112107, 2020.

[111] A. B. Pun, S. N. Sanders, M. Y. Sfeir, L. M. Campos, and D. N. Congreve. Annihilator dimers enhance triplet fusion upconversion. *Chemical Science*, 10(14):3969–3975, 2019.

[112] C. Gao, S. K. K. Prasad, B. Zhang, M. Dvořák, M. J. Y. Tayebjee, D. R. McCamey, T. W. Schmidt, T. A. Smith, and W. W. H. Wong. Intramolecular Versus Intermolecular Triplet Fusion in Multichromophoric Photochemical Upconversion. *The Journal of Physical Chemistry C*, 123(33):20181–20187, 2019.

[113] C. J. Imperiale, P. B. Green, E. G. Miller, N. H. Damrauer, and M. W. B. Wilson. Triplet-Fusion Upconversion Using a Rigid Tetracene Homodimer. *The Journal of Physical Chemistry Letters*, 10(23):7463–7469, 2019.

[114] A. Olesund, V. Gray, J. Mårtensson, and B. Albinsson. Diphenylanthracene Dimers for Triplet–Triplet Annihilation Photon Upconversion: Mechanistic Insights for Intramolecular Pathways and the Importance of Molecular Geometry. *Journal of the American Chemical Society*, 143(15):5745–5754, 2021.

[115] A. Ronchi and A. Monguzzi. Developing solid-state photon upconverters based on sensitized triplet–triplet annihilation. *Journal of Applied Physics*, 129(5):050901, 2021.